The Meteoritical Society

Meteoritics & Planetary Science 1–23 (2023)
doi: 10.1111/maps.14043

The bulk mineralogy, elemental composition, and water content of the Winchcombe CM chondrite fall

H. C. BATES[1]*, A. J. KING[1], K. S. SHIRLEY[2], E. BONSALL[3], C. SCHRÖDER[3], F. WOMBACHER[4], T. FOCKENBERG[5], R. J. CURTIS[2], and N. E. BOWLES[2]

[1]Planetary Materials Group, Natural History Museum, London, UK
[2]Atmospheric, Oceanic and Planetary Physics, University of Oxford, Oxford, UK
[3]Biological and Environmental Sciences, Faculty of Natural Sciences, University of Stirling, Stirling, UK
[4]Institut für Geologie und Mineralogie, Universität zu Köln, Köln, Germany
[5]Institut für Geologie, Mineralogie und Geophysik, Ruhr-Universität Bochum, Bochum, Germany
***Correspondence**
H. C. Bates, Planetary Materials Group, Natural History Museum, Cromwell Road, London SW7 5BD, UK.
Email: h.bates@nhm.ac.uk

(Received 14 June 2022; revision accepted 17 June 2023)

Abstract–On the microscale, the Winchcombe CM carbonaceous chondrite contains a number of lithological units with a variety of degrees of aqueous alteration. However, an understanding of the average hydration state is useful when comparing to other meteorites and remote observations of airless bodies. We report correlated bulk analyses on multiple subsamples of the Winchcombe meteorite, determining an average phyllosilicate fraction petrologic type of 1.2 and an average water content of 11.9 wt%. We show the elemental composition and distribution of iron and iron oxidation state are consistent with measurements from other CM chondrites; however, Winchcombe shows a low Hg concentration of 58.1 ± 0.5 ng g^{-1}. We demonstrate that infrared reflectance spectra of Winchcombe are consistent with its bulk modal mineralogy, and comparable to other CM chondrites with similar average petrologic types. Finally, we also evaluate whether spectral parameters can estimate H/Si ratios and water abundances, finding generally spectral parameters underestimate water abundance compared to measured values.

INTRODUCTION

The Winchcombe fireball was observed at 21:54:16 (UT) on 28 February 2021. A total of 535 g of meteoritic material was recovered over the following 7 days, with a further ~100 g found within 4 weeks (King et al., 2022; Russell et al., 2022). Initial petrologic characterization of the Winchcombe meteorite found heavily altered chondrules, chondrule pseudomorphs, and calcium-aluminium-rich inclusions (CAIs) set in a fine-grained matrix consisting of Fe- and Mg-bearing phyllosilicates, tochilinite–cronstedtite intergrowths (TCIs), carbonates, magnetite, and sulfides (MB 110, King et al., 2022; Suttle et al., 2022). The initial bulk elemental abundances and oxygen, titanium, and chromium isotopic compositions are consistent with Winchcombe being a CM carbonaceous chondrite (MB 110, Greenwood et al., 2022; King et al., 2022).

The CM chondrites typically record low-temperature (<250°C) aqueous alteration on their parent asteroids within the first 10 Myr of solar system formation (Benedix et al., 2003; Clayton & Mayeda, 1984; Fujiya et al., 2012; Guo & Eiler, 2007; Jilly et al., 2014; Tomeoka & Buseck, 1985; Vacher et al., 2019; Visser et al., 2020). Some CM chondrites experienced moderate aqueous alteration (CM2.5–2.2 on the Rubin et al., 2007 petrologic scale), whereas others underwent near complete hydration (CM2.1–2.0) (Browning et al., 1996; Grady et al., 1987; Howard et al., 2015; King et al., 2017; Kojima et al., 1984; Lentfort et al., 2021; McSween, 1979; Rubin et al., 2007; Zolensky et al., 1997). The record of variable aqueous alteration in CM chondrites can indicate the conditions on the CM parent body/bodies; such as differences in water/rock ratios, temperatures, and duration of alteration (Fujia, 2018; Guo & Eiler, 2007;

Howard et al., 2015; King, Mason, et al., 2021; Palguta et al., 2010; Vacher et al., 2019; Verdier-Paoletti et al., 2017, 2019). Winchcombe in particular gives a unique opportunity to investigate aqueous alteration due to its status as one of the quickest recovered meteoritic falls, with the first samples being collected within 12 h of the fireball, therefore minimizing the influence of terrestrial alteration (Jenkins et al., 2022; Russell et al., 2022).

On a millimeter scale, Winchcombe is a breccia containing several lithologies that record different degrees of alteration. Nevertheless, bulk properties are useful for understanding average alteration, and correlated analyses of relatively large amounts of sample can be used to reconstruct alteration history. Having a measure of average composition and alteration is valuable when comparing to remote observations of asteroids. In the case of samples returned from asteroids Ryugu and Bennu by JAXA's Hayabusa2 and NASA's OSIRIS-REx missions, we can directly compare lithologies between meteorites and the asteroid samples. However, a majority of asteroids remain unsampled, and the only data available are broad averages of surface composition, and hence alteration. The best comparison to these observations is evaluations of average composition and alteration from meteorites. Here, we provide further interpretations of the degree of aqueous alteration of the Winchcombe meteorite, by showing results from a collaborative investigation of its bulk-scale properties, using x-ray diffraction (XRD), thermogravimetric analysis (TGA), Karl-Fischer titration, Mössbauer spectroscopy, and element analyses using inductively coupled plasma mass spectroscopy (ICP-MS) and a mercury analyzer. We also provide an interpretation of the infrared spectra initially presented in King et al. (2022), by comparing spectral parameters to trends established for differing bulk mineralogy and degrees of aqueous alteration in CM chondrites. Our aim was to establish the average alteration history of Winchcombe and determine its relationship with other CM chondrites and potential asteroid parent bodies.

SAMPLES AND METHODS

Samples

A total of nine subsamples of Winchcombe were investigated for this study, the details of which are summarized in Table 1. Briefly, most samples investigated here were collected from the driveway of the Wilcock family in Winchcombe: samples with the registration number BM.2022,M1 were collected on March 1, 2021; BM.2022, M2 samples were collected on March 3, 2021; BM.2022,M3 samples were collected on March 4, 2021; and BM.2022,M4 samples were collected on March 5, 2021. The subsample with the registration number BM.2022,M8 was collected from a locality in Woodmancote by the Mounsey family on March 5, 2021. The Winchcombe samples collected on the 1st, 3rd, and 4th of March were transported to the Natural History Museum, London (NHM) on the 4th of March, before being sealed in glass vials stored within polyethylene samples bags. These were stored in a bench-top desiccator. The samples collected on the 5th of March were transported to the NHM on the 8th of March and subjected to the same storage conditions. As much as possible, these vials are not opened, so as to reduce terrestrial contamination, and when measurements are carried out, the vials are opened only shortly before preparation and analysis. For further details on the Winchcombe recovery and storage, see King et al. (2022) and Russell et al. (2022).

PSD-XRD

King et al. (2022) reported mineral abundances for two Winchcombe samples; BM.2022,M2-41 and BM.2022,M1-91. Here, we report mineral abundances for two further samples; BM.2022,M4-7 and BM.2022,M1-22.

Modal mineral abundances were determined using position-sensitive detector x-ray diffraction (PSD-XRD) at the Natural History Museum, London (NHM). Each sample was ground to a particle size of <50 μm using an agate mortar and pestle. Approximately 50 mg of powdered sample was packed into an aluminum sample well with the sharp edge of a stainless steel spatula and analyzed using an Enraf-Nonius PDS120 x-ray diffractometer with an INEL-curved 120° PSD. The PSD was in a static geometry relative to the x-ray beam and sample stage, the latter of which was rotated continuously throughout an analysis. Cu $K\alpha_1$ radiation was selected using a Ge 111 monochromator and the size of the beam on the sample was restricted to 0.24×2.00 mm using post-monochromator slits. The beam flux of the instrument was monitored at regular intervals using a polished Fe-metal block and varied $<1\%$ over the experimental run. Diffraction patterns were collected from the meteorite samples for 16 h and from mineral standards prepared in the same way for 30 min.

Mineral abundances were determined using a profile-stripping technique (Cressey & Schofield, 1996), following the same procedure which has been used to investigate the mineralogy of CI, CM, CO, CV, CR, and CY chondrites (Alexander et al., 2018; Bates et al., 2021; Bland et al., 2004; Hanna et al., 2020; Howard et al., 2009, 2011, 2015; King, Schofield, et al., 2015; Lee et al., 2016). Previous studies using the profile-stripping method have applied a linear least-squares routine to fit the standard patterns to the meteorite patterns in order to determine detection limits and uncertainties in mineral

TABLE 1. Samples used in this study.

BM registration number	Mass (g)	PSD-XRD (with modal mineralogy)	PSD-XRD	TGA	Karl-Fischer	Mössbauer	Mercury	ICPMS	Measurements in other studies
BM.2022,M4-7	0.3111	x	x						
BM.2022,M1-22	2.0051	x	x	x					Goniometer (Curtis et al., 2023; King et al., 2022)
BM.2022,M3-4	0.1387		x			x			
BM.2022,M1-100	0.0050					x			
BM.2022,M3-27	0.0240					x			
BM.2022,M8-14	0.0040					x			
BM.2022,M1-97	0.0898				x		x	x	
BM.2022,M2-41	0.2800			x					IR reflectance spectroscopy, PSD-XRD, bulk chemistry (King et al., 2022)
BM.2022,M1-91	0.2700			x					IR reflectance spectroscopy, PSD-XRD, bulk chemistry (King et al., 2022)

Note: For collection information for each British Museum (BM) registration number, see table S4 in King et al. (2022).

abundances (King, Schofield, et al., 2015; Schofield et al., 2002). This process found similar mineral standard factors that were identified in the profile-stripping method and yielded detection limits of 0.5–1 vol% and absolute uncertainties in the abundances of 1–1.5 vol%.

To further characterize the mineralogy of the Winchcombe meteorite, small aliquots (~1–2 mg) of powdered samples BM.2022,M3-4 and BM.2022,M4-7 were mounted using acetone as a smear on low-background single crystal sapphire substrates. XRD patterns were then collected from the samples using the PSD-XRD and Cu $K\alpha_1$ radiation. Silicon and silver behenate were used to calibrate the instrument and phases in the meteorite samples were identified using the International Centre for Diffraction Data (ICDD) database (PDF-2).

Water Content by TGA

The water content of samples BM.2022,M1-22; BM.2022,M1-91; and BM.2022,M2-41 was estimated by thermogravimetric analysis (TGA). The latter two samples were measured on May 6, 2021 and BM.2022, M1-22 was measured on August 6, 2021. Approximately 10–15 mg of each powdered sample was analyzed using a TA Instruments Simultaneous Thermal Analysis (SDT) Q600 at the NHM. For analysis, the powder was loaded into an alumina crucible and placed onto the TGA balance. Mass loss was then recorded as the sample was heated in a sealed furnace from room temperature (~20–25°C) to 1000°C at 10°C min^{-1} under an N_2 flow of 100 mL min^{-1}. The sensitivity of the TGA balance is 0.1 μg and the overall error on the measured mass loss fractions is ~0.1% (King, Solomon, et al., 2015).

Water Content by Karl-Fischer Titration

Sample BM.2022,M1-97 (89.9 mg) was powdered using an agate mortar and pestle. The water content of a small aliquot (4.5 mg) was then determined by Karl-Fischer Titration at the Institute for Geology, Mineralogy and Geophysics at the Ruhr-University Bochum. For comparison, and to test the repeatability of the technique for CM samples, a sample of the CM chondrite fall Murchison (USNM 5450) was analyzed at the same time. Prior to analysis, the Winchcombe and Murchison powders were heated to 110°C for 3 h and then stored in a desiccator. Water analyses were then performed using a Mitsubishi CA 200 moisture meter (e.g., Bischoff et al., 2021). To this end, about 3–5 mg of powder aliquots was heated in a high-frequency induction furnace to 1000°C. The liberated water was conducted into the titration cell, where the water content was determined by the Karl-Fischer method. The instrument was tested with an internal laboratory standard (5 wt% H_2O) prior to and after the measurements which yields an intermediate precision of ±0.5 wt% water (2 sd).

Mercury

The determination of Hg employed a Milestone DMA-80 Hg analyzer at the Institut für Geologie und Mineralogie at the Universität zu Köln, Germany. Two aliquots of 10.6 and 16.5 mg of the powdered sample BM.2022,M1-97 were heated in an oven to 750°C and the liberated Hg carried by an O_2 gas stream to a gold amalgamator. The amalgamator was then heated to liberate the Hg into an atomic absorption spectrometer. Prior to the analyses, the instrument was calibrated using dilutions from a NIST SRM 3133 Hg solution and a Merck-Supelco Hg standard solution. Our in-house rock standard yields a repeatability of ±0.5 ng g^{-1} (n = 13) at 27.0 ng g^{-1}.

Element Analysis by ICP-MS

A 52.6 mg aliquot of the powdered sample BM.2022, M1-97 plus the CM chondrites, Murchison and Paris, were analyzed for their chemical composition by ICP-MS. For each sample, approximately 50 mg of powder was weighed into 15 mL PFA beakers to which 1.5 mL of 24 M HF and 1.5 mL 14 M HNO_3 were added. The beakers were capped and placed into Parr pressure digestion vessels and heated in an oven for 72 h at 180°C. Three milliliters of 14 M HNO_3 was added to the sample solutions, before they were dried down for the first time at 120°C on a hotplate. In order to further drive off excess HF and prevent insoluble fluoride formation, 5 mL of 14 M HNO_3 was added via pipette, the solution was refluxed in capped beakers at 120°C on the hotplate for several hours (typically overnight), and again dried down at 120°C. The latter step was repeated two more times. To successfully prevent the formation of insoluble fluorides, dry down steps were always watched to ensure that sample cakes stayed moist until the final dry down step. About 5 µg of the internal standard elements Rh and Re was then added in 250 µL of 0.28 M HNO_3 via pipette and the weight of the internal standard solution precisely recorded. The sample cakes were redissolved and diluted to achieve 4000-fold dilutions in 0.28 M HNO_3 for analyses.

Analyses were carried out using the iCAP Q at the Institut für Geologie und Mineralogie at the Universität zu Köln, Germany, equipped with an ESI SC-2 DX autosampler, a self-aspirating PFA nebulizer (approximately 100 mL min^{-1} uptake), and a Peltier cooled cyclonic PFA spray chamber. Only Se, Rb, Y, Zr, Nb, Ag, In, and Ba were analyzed in STD mode (no cell use), and all other elements were analyzed in KED (kinetic energy discrimination) mode. Each sample was analyzed within at least four measurement sessions. Two sessions utilized He, two other sessions used 5% H_2 in He as a cell gas in KED mode and for both cases, more sensitive 2.8 or more robust 3.5 mm skimmer cone insets were used once. There was no systematic difference in any of the results and all data were pooled together. Two values of W in Murchison were rejected as obvious outliers.

Sensitivity and interference rates were checked for each session using a 1 ng mL^{-1} Co, In, Ba, and Ce tune solution (where two values are given, the first refers to the 3.5 mm skimmer cone inset, the second to 2.8 mm insets): STD mode yielded 105,000 or 179,000 cps for ^{115}In; 50,000 or 88,000 cps for ^{59}Co; CeO/Ce = 0.7 or 1.0% and Ba++/Ba+ = 5%; KED mode yielded 20,000 or 33,000 cps for ^{59}Co; CeO/Ce = 0.3% and Ba++/Ba+ = 8%.

Matrix-matched external calibration utilized three homemade reference solutions slightly modified from those used in Braukmüller et al. (2018). The Ga data are based on a one-point calibration. For drift correction, Rh was used as an internal standard for ^{135}Ba and lower mass analyte isotopes; Re was used for all heavier ones. All data reported were clearly above the quantification limit, as calculated from repeated background sample solution measurement signals + 10 standard deviations. Meteorite analyses were accompanied by four procedure blanks. These were fairly reproducible and average blank values were subtracted. However, blank contributions to the sample signals were negligible; by far the largest blank contribution amounted to 1.8 ± 0.3% for W.

Mössbauer

Four samples of the Winchcombe meteorite, one powder sample and three rock chips, were investigated at the Mössbauer Spectroscopy laboratory for Earth and Environment (MoSEE) at the University of Stirling. The entire 138.7 mg powdered sample (BM.2022,M3-4) was transferred into an acrylic glass sample holder (~1.3 cm circular diameter) and measured at three different temperatures (room temperature, 77 and 4.2 K) with a standard Wissenschaftliche Elektronik transmission spectrometer attached to an ICEoxford Dry ICE 4 K closed-cycle helium gas cryostat.

The rock chips were measured without any further sample preparation at room temperature with a miniaturized Mössbauer spectrometer MIMOS II (Klingelhöfer et al., 2003), which is set up in backscattering geometry. Both instruments use 14.4 keV gamma radiation emitted by a ^{57}Co in rhodium matrix source. The radiation source was in constant acceleration mode (triangular waveform). Meteorite spectra were calibrated against that of alpha-iron foil (25 µm thickness) at room temperature.

Transmission spectra were evaluated with Recoil software using Lorentzian line profiles. Backscatter spectra were evaluated with an in-house software routine

(Mbfit) using Lorentzian line profiles. Mbfit is based on the least-squares minimization routine MINUIT (James, 2004). No *f*-factor correction was applied.

RESULTS

Mineral Identification and Abundance

Figure 1 shows the PSD-XRD patterns collected from the BM2022,M4-7 and BM.2022,M3-4 Winchcombe samples prepared as smears on a sapphire substrate. The PSD-XRD patterns for samples BM2022, M4-7 and BM.2022,M1-22 which were prepared as powders packed into aluminum wells show the same diagnostic peaks. The crystalline phases identified are olivine, magnetite, tochilinite carbonate (calcite), sulfate (gypsum), and sulfides (pyrrhotite). We observe diffraction peaks in all patterns at ~12° and ~25°, and much broader features at ~19° and ~61°. Howard et al. (2009, 2011) interpreted these peaks as arising from relatively crystalline Fe-rich serpentine and fine-grained, poorly crystalline Mg-Fe serpentine, respectively.

We were able to quantify modal mineralogy for BM2022,M4-7 and BM.2022,M1-22. Both enstatite and gypsum were each identified in sample BM.2022,M4-7 at an abundance of 1 vol%. As this sample was collected on March 5, 2021 (5 days after the fireball was observed), the gypsum may be a terrestrial weathering product. Tochilinite was identified from a low intensity peak ~16° in all patterns, although we are unable to quantify its abundance as we do not have a pure standard of sufficient mass available for the profile stripping. However, as the peak is small and the final residual for the Winchcombe samples still reached zero counts, we account for the tochilinite through the subtraction of the Fe-cronstedtite and/or Mg-serpentine standards and confirm that its abundance is probably <1 vol%.

The modal mineralogy of both samples is summarized in Table 2. A petrologic type based on the phyllosilicate fraction (PSF) can be determined from the modal mineralogy. This expresses the degree of aqueous alteration as the volume of phyllosilicates divided by the abundance of phyllosilicates plus total anhydrous silicates. This gives a petrologic type, with a PSF of <0.05 as type 3.0 and >0.95 as type 1 (Howard et al., 2015). Sample BM.2022,M4-7 has a PSF petrologic type of 1.3 and sample BM.2022,M1-22 is 1.2.

Abundance of Water/OH

Figure 2 shows the mass loss and DTG curves for the Winchcombe samples BM.2022,M1-91. Curves for BM.2022,M1-22 and BM.2022,M2-41 are very similar (Figure S1). Previous studies of hydrated carbonaceous chondrites have divided TGA curves into distinct temperature regions: mass loss <100°C is attributed to the removal of adsorbed terrestrial water, from 100 to 200°C mainly to the breakdown of sulfates; between 200–400 and 400–770°C due to the release of $-OH/H_2O$ in Fe-(oxy)hydroxides and phyllosilicates, respectively; and between 770 and 900°C from CO_2 produced during the breakdown of carbonates (Garenne et al., 2014; King, Solomon, et al., 2015). Additional mass loss in these temperature ranges could also result from the decomposition of Fe-sulfides and refractory organic matter, present in CM chondrites at ~1–2 wt% (Alexander et al., 2007), although the contribution is expected to be small. We do not observe any significant evidence for sulfate dehydration, which supports the meteorite having little terrestrial contamination at the time of measurement. Mass loss between 200 and 770°C is assumed to be due to water and Garenne et al. (2014) showed that water abundances derived from TGA, although often slightly higher, correlate well with those measured using other analytical methods.

The mass loss at different temperature ranges is summarized in Table 3. Assuming all mass loss between 200 and 770°C is due to dehydration and dehydroxylation of phyllosilicates, we obtain water abundances of 12.9, 13.3, and 12.4 wt%.

In addition, five repeated analyses of the Murchison CM2 chondrite conducted in July 2020 and October 2021 yielded water contents determined through Karl-Fischer titration of 11.1 ± 0.3 wt% (2 sd). Assuming that the same precision applies to Winchcombe, a single measurement of water abundance calculated through Karl-Fischer titration yields 13.8 ± 0.3 wt% H_2O.

Element Composition

Two analyses of Winchcombe yielded 57.5 and 58.5 ng g^{-1} Hg, respectively. Thus, an average Hg concentration and estimated uncertainty ("Mercury" Section) of 58.1 ± 0.5 ng g^{-1} was obtained for sample BM.2022,M1-97.

The ICP-MS data for Winchcombe, Murchison, and Paris are reported as μg g^{-1} in Table 4, along with the repeatability given as the absolute and relative (in %) doubled standard deviation. For most elements, the repeatability is excellent, typically below 5% and around 1% for many major elements. Figure 3 shows quadrupole ICP-MS data for Winchcombe, Murchison, and Paris, normalized to Mg and CI chondrite reference values.

Mössbauer Analyses

The MIMOS II instrument enabled nondestructive analyses of the Winchcombe samples BM.2022,M1-100; BM.2022,M3-27; and BM.2022,M8-14. Initially, the

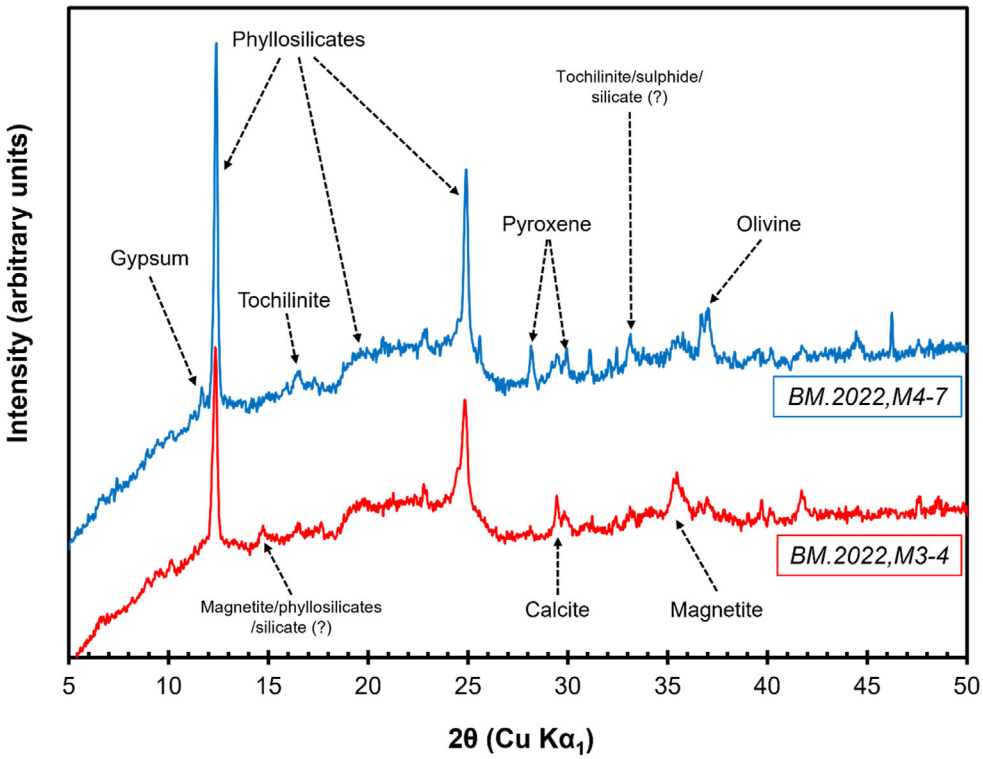

FIGURE 1. PSD-XRD patterns collected from samples of BM.2022,M4-7 and BM.2022,M3-4 prepared as smears on low background substrates. Measurement times were ~9 h for BM.2022,M4-7 and ~2 h for BM.2022,M3-4.

TABLE 2. Modal mineralogy of Winchcombe as determined through PSD-XRD.

Sample	Olivine (vol%)	Enstatite (vol%)	Magnetite (vol%)	Carbonate (vol%)	Sulfide (vol%)	Sulfate (vol%)	Mg-serpentine (vol%)	Fe-cronstedtite (vol%)	PSF petrologic type
BM.2022,M4-7	8	2	1	1	1	1	57	29	1.3
BM.2022,M1-22	6	–	5	1	<1	–	47	41	1.2

Note: See the main text for details on the PSF petrologic type.

velocity range ± 12 mm s^{-1} was measured (Figure S2); however, as the spectra did not indicate the presence of magnetically ordered compounds whose sextet lines would appear in the outer velocity reaches of the Mössbauer spectrum, the maximum velocity was reduced from ±12 to ±4.5 mm s^{-1}. This increased the spectral resolution across the central peaks. We added up the counts from the measurements of the three Winchcombe chips and fitted the resultant summed spectrum. We used the parameters obtained (Table 5) to then find the subspectral area for each mineral phase, the value of which is proportional to the amount of iron in that mineral phase (Figure 4; Table 6). Abundances are shown as percentage of total iron.

Temperature-dependent transmission spectra were obtained from the powdered BM.2022,M3-4 sample (Figure 5). For consistency, we used the same parameters obtained for the rock chip spectra (Table 5) and added magnetite parameters from the literature (Cornell & Schwertmann, 2003) to fit the room temperature spectrum and determine the amount of iron in each mineral phase (Figure 5, top panel; Table 6). Mössbauer parameters change with temperature, and the 77 K spectrum thus needed to be fitted independently (Figure 5; Table 7). Diamagnetic and paramagnetic mineral phases manifest in a Mössbauer spectrum as a single line (singlet) or double line (doublet). Below the magnetic ordering temperature of paramagnetic phases, the spectral pattern becomes a six-line spectrum (sextet). Magnetic ordering is apparent in the 4.2 K spectrum, but the spectrum is too complex to be fitted without any further constraints. We therefore only highlighted the locations of peaks characteristic for specific mineral phases (Figure 5).

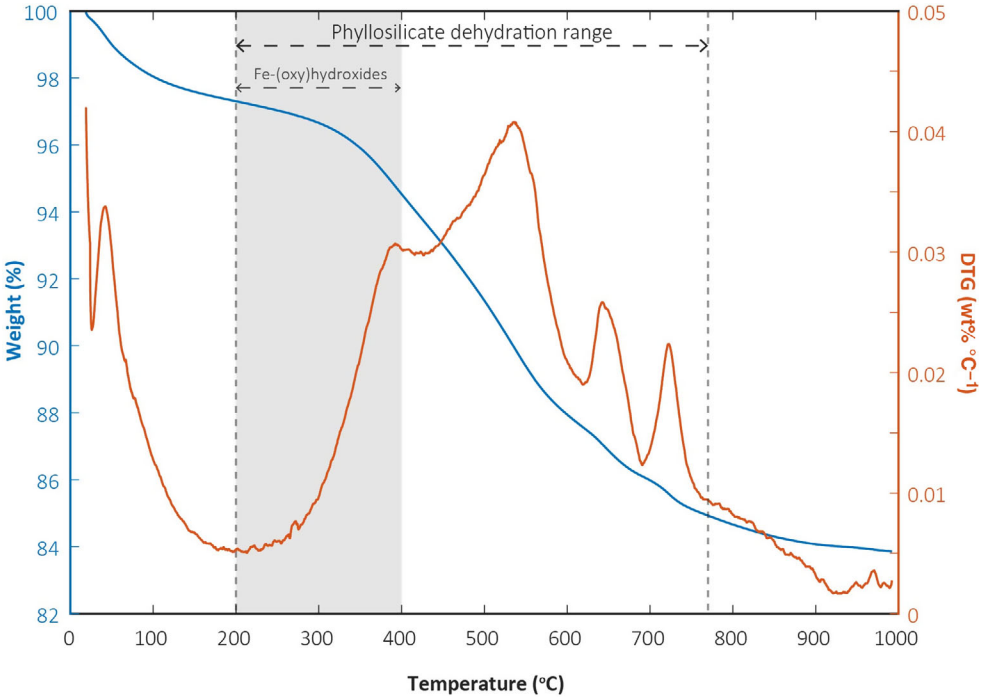

FIGURE 2. Mass loss and derivative of mass loss (DTG) curves for the Winchcombe sample BM.2022,M1-91. Peaks in the DTG curves correspond to specific mineral phases dehydrating or breaking down. Winchcombe shows significant mass loss between 200 and 770°C due to the dehydration and dehydroxylation of phyllosilicates; however, small amounts of Fe-(oxy) hydroxides, Fe-sulfides, and some organic matter may also contribute to mass loss in this region.

TABLE 3. Mass loss (wt%) as a function of temperature during TGA of the Winchcombe meteorite samples.

Sample	25–200°C	200–400°C	400–770°C	770–900°C	H_2O (200–770°C)	Fe-serpentine (300–450°C)	Mg-serpentine (450–800°C)	PSF classification
BM.2022,M1-22	3.4	2.7	10.2	0.9	12.9	3.9	8.8	1.3
BM.2022,M2-41	3.0	3.7	9.7	0.5	13.3	4.2	8.1	1.1*
BM.2022,M1-91	2.7	2.8	9.6	0.9	12.4	3.6	8.4	1.2*

Note: The DTG curve is divided into temperature regions related to the dehydration of terrestrial adsorbed H_2O (15–200°C), the dehydration and dehydroxylation of Fe-(oxy)hydroxides (200–400°C) and phyllosilicates (400–770°C), and the breakdown of carbonates (770–900°C). The starred values of PSF petrologic type for BM.2022,M2-41 and BM.2022,M1-91 were determined in King et al. (2022).

DISCUSSION

Modal Mineralogy and Water Content

Winchcombe multiple lithologies with different petrologic types (King et al., 2022; Suttle et al., 2022). However, it can be challenging to accurately characterize the fine-grained mineralogy, so it can be useful to consider the degree of alteration on a bulk scale. Additionally, bulk properties are better comparisons to remote observations, as heterogeneity at the micron scale is difficult to determine from telescopic or spacecraft observations.

PSD-XRD has been used to investigate the modal mineralogy of a number of different meteorite types and lithologies (Alexander et al., 2018; Bischoff et al., 2021; Bland et al., 2004; Hanna et al., 2020; Howard et al., 2009, 2011, 2015; Kerraouch et al., 2022; King, Bates, et al., 2019; King, Russell, et al., 2019; King, Schofield, et al., 2015, 2021; Lee et al., 2016). Howard et al. (2009) showed in the case of CM chondrites that the bulk mineralogy of different subsamples (~50–200 mg) of the same meteorite often varies by <5 vol%. The bulk PSF petrologic type for the two samples in this study is 1.2 and 1.3, which in the Rubin et al. (2007), petrologic scale corresponds to 2.1 and 2.2. These

TABLE 4. Chemical composition of Winchcombe, Murchison, and Paris CM2 chondrites determined by ICP-MS.

	Winchcombe (n = 4)			Murchison (n = 11)			Paris (n = 7)		
	μg g^{-1}	2 sd	2 rsd (%)	μg g^{-1}	2 sd	2 rsd (%)	μg g^{-1}	2 sd	2 rsd (%)
Na	5097	28	0.6	3879	45	1.2	4466	63	1.4
Mg	116,415	650	0.6	116,578	1627	1.4	117,757	1402	1.2
Al	11,226	78	0.7	11,160	203	1.8	11,134	102	0.9
P	1021	30	2.9	988	35	3.6	975	24	2.4
S	31,591	440	1.4	30,528	1147	3.8	32,493	755	2.3
K	425	11	2.6	390	14	3.5	390	9	2.2
Ca	12,242	72	0.6	12,269	158	1.3	13,083	82	0.6
Sc	7.72	0.13	1.7	8.08	0.15	1.9	8.13	0.11	1.4
Ti	560.8	5.0	0.9	567.7	7.5	1.3	570.5	4.9	0.9
V	69.20	0.61	0.9	69.52	0.84	1.2	70.00	0.46	0.7
Cr	3059	20	0.6	3037	25	0.8	3026	27	0.9
Mn	1726	9	0.5	1659	35	2.1	1657	17	1.0
Fe	211,368	1255	0.6	206,941	1473	0.7	204,830	2358	1.2
Co	587.9	5.0	0.8	575.5	7.4	1.3	564.1	5.1	0.9
Ni	12,649	50	0.4	12,389	93	0.8	12,148	123	1.0
Cu	133.5	0.9	0.7	125.9	1.3	1.1	126.8	1.0	0.8
Zn	182.7	4.1	2.2	182.3	5.5	3.0	183.3	4.2	2.3
Ga	7.85	0.19	2.4	7.47	0.19	2.5	7.37	0.22	3.0
As	1.829	0.055	3.0	1.751	0.049	2.8	1.723	0.055	3.2
Se	13.0	1.0	7.8	13.1	0.7	5.2	13.1	0.8	5.9
Rb	1.721	0.017	1.0	1.626	0.022	1.3	1.675	0.026	1.6
Y	1.864	0.020	1.1	1.889	0.020	1.1	1.885	0.015	0.8
Zr	4.772	0.040	0.8	4.735	0.072	1.5	4.721	0.079	1.7
Nb	0.3546	0.0078	2.2	0.3620	0.0063	1.8	0.3553	0.0088	2.5
Ag	0.1219	0.0032	2.6	0.1230	0.0062	5.1	0.1284	0.0056	4.4
Cd	0.386	0.007	1.8	0.396	0.018	4.6	0.391	0.015	3.9
In	0.0453	0.0021	4.5	0.0456	0.0022	4.8	0.0472	0.0014	2.9
Cs	0.1065	0.0088	8.3	0.1210	0.0058	4.8	0.1450	0.0031	2.1
Ba	3.462	0.058	1.7	2.998	0.068	2.3	2.941	0.087	3.0
La	0.294	0.010	3.4	0.296	0.005	1.8	0.294	0.010	3.3
Ce	0.776	0.014	1.8	0.784	0.006	0.8	0.774	0.016	2.0
Pr	0.1196	0.0013	1.1	0.1215	0.0025	2.0	0.1194	0.0031	2.6
Nd	0.621	0.012	1.9	0.626	0.019	3.1	0.621	0.026	4.1
Sm	0.202	0.020	9.8	0.204	0.010	4.9	0.203	0.008	3.8
Eu	0.0778	0.0064	8.2	0.0775	0.0028	3.6	0.0765	0.0037	4.9
Gd	0.2743	0.0037	1.4	0.2784	0.0109	3.9	0.2784	0.0084	3.0
Tb	0.0501	0.0012	2.3	0.0509	0.0018	3.6	0.0501	0.0015	2.9
Dy	0.3417	0.0069	2.0	0.3439	0.0091	2.6	0.3438	0.0094	2.7
Er	0.2157	0.0074	3.4	0.2190	0.0057	2.6	0.2193	0.0048	2.2
Tm	0.0340	0.0009	2.6	0.0342	0.0014	4.0	0.0340	0.0011	3.1
Yb	0.2249	0.0064	2.8	0.2298	0.0065	2.8	0.2299	0.0076	3.3
Lu	0.0345	0.0016	4.5	0.0338	0.0015	4.6	0.0332	0.0010	3.0
Hf	0.1432	0.0055	3.9	0.1365	0.0050	3.7	0.1349	0.0052	3.8
W	0.097	0.006	6.5	0.101	0.003	3.1	0.103	0.006	5.5
Ir	0.5011	0.0033	0.7	0.5375	0.0098	1.8	0.4637	0.0083	1.8
Pt	1.046	0.026	2.4	1.092	0.020	1.8	1.053	0.018	1.7
Tl	0.0813	0.0042	5.1	0.0819	0.0028	3.4	0.0812	0.0030	3.7
Th	0.0356	0.0014	3.9	0.0365	0.0013	3.7	0.0354	0.0013	3.7

petrologic types are consistent with those reported by King et al. (2022) for three further subsamples of Winchcombe (BM.2022,M2-41; BM.2022,M1-91; and BM.2022,M2-36; PSF = 1.1–1.2). On a bulk scale, the Winchcombe meteorite is one of the most aqueously altered CM chondrite falls, which is emphasized in Figure 6, which shows that as the degree of aqueous alteration in CM chondrites increases, silicate abundance

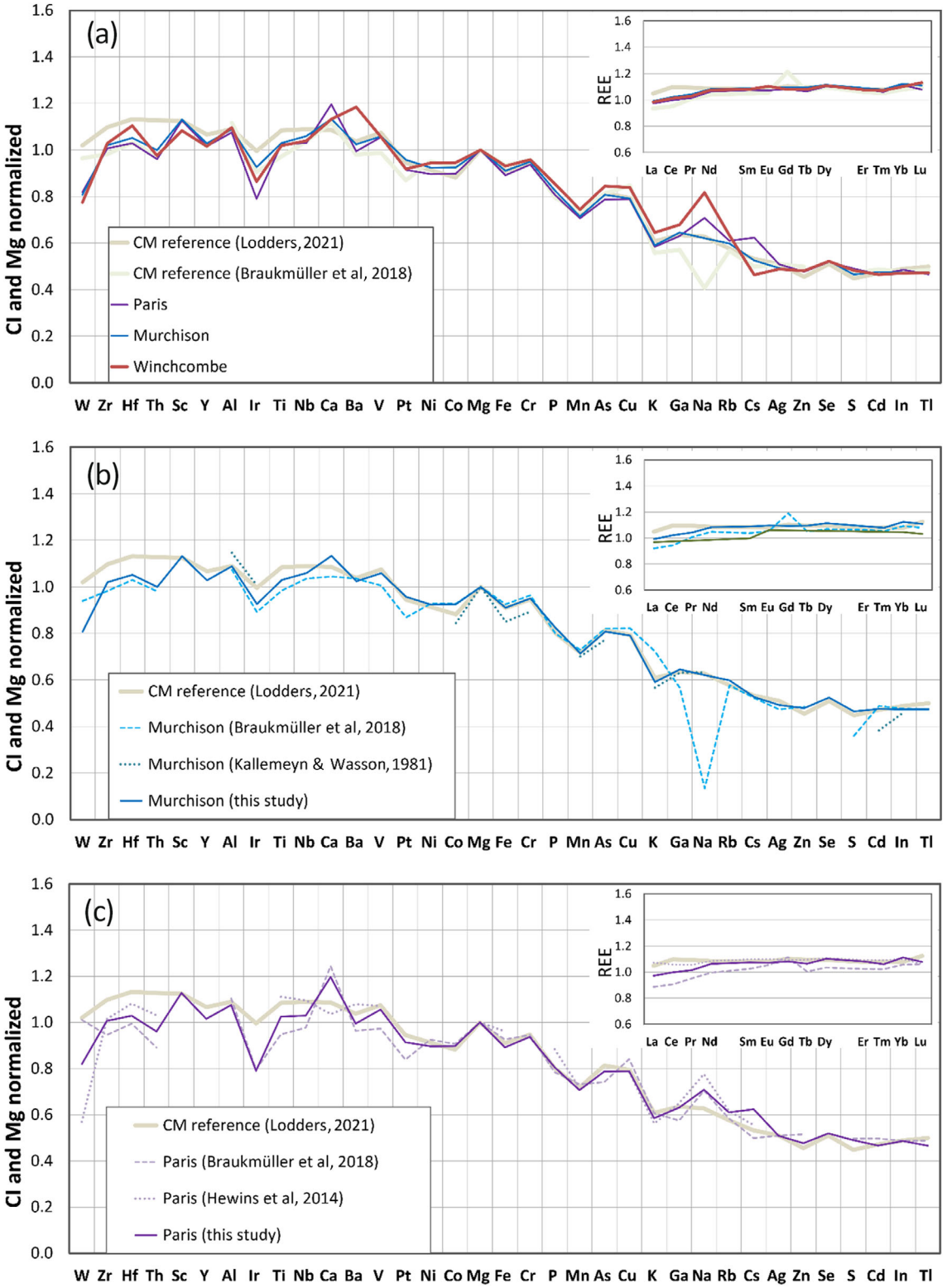

FIGURE 3. (a) Quadrupole ICP-MS data for Winchcombe, Murchison and Paris CM2 chondrites normalized to Mg and CI reference values from Lodders (2021) ordered by decreasing 50% condensation temperatures (Kiseeva & Wood, 2015; Lodders, 2003); REE data in inset ordered by atomic number. CM chondrite reference values are from Lodders (2021) and Braukmüller et al. (2018). Comparison of CI and Mg normalized data with literature data for Murchison (b) and Paris (c), respectively.

TABLE 5. Mössbauer parameters used to fit room temperature spectra.

Mineral phase	Fe ox. state and coordination	δ (mm s^{-1})	ΔE_Q or ε (mm s^{-1})	B_{hf} (T)	Γ (HWHM) (mm s^{-1})
Cronstedtite	Fe^{2+}	1.10	2.64	–	0.17
	Fe^{3+} tetrahedral	0.29	0.36	–	0.15
	Fe^{3+} octahedral	0.32	0.76	–	0.14
Serpentine	Fe^{2+}	1.11	2.09	–	0.25
Tochilinite	Fe^{2+}	0.49	0.85	–	0.33
Magnetite	$Fe^{2.5+}$octahedral	0.26	0.01	49	0.20
	Fe^{3+} tetrahedral	0.67	0.00	46	0.20

Note: Magnetite parameters are from Cornell and Schwertmann (2003). δ, isomer shift; ΔE_Q, quadrupole split; ε, quadrupole shift; B, magnetic hyperfine field; Γ, half width at half maximum for the relevant peak.

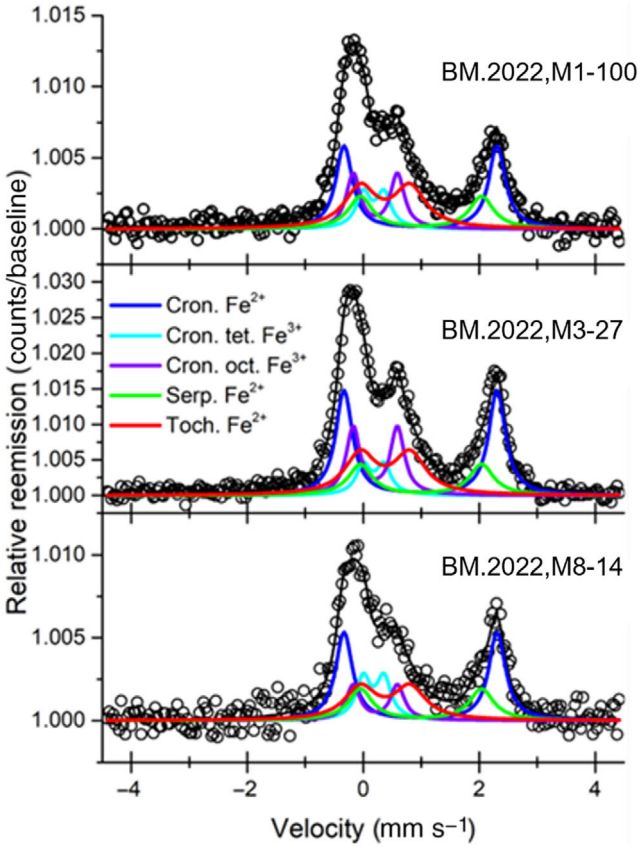

FIGURE 4. Backscatter Mössbauer spectra of three rock chips of the Winchcombe meteorite obtained at room temperature with the miniaturized Mössbauer spectrometer MIMOS II over a reduced velocity range. Black solid line represents the overall fit to the measured (black open circles) and is the sum of all subspectra (colored lines). Cronstedtite (Cron.) contains Fe^{2+} and Fe^{3+}, the latter in tetrahedral (tet.) and octahedral (oct.) coordination. Serpentine (Serp.) and tochilinite (Toch.) contain Fe^{2+}.

decreases and phyllosilicate abundance increases. Other recent CM falls which show a similar modal mineralogy are Kolang (King, Bates, et al., 2021) and Mukundpura (Krietsch et al., 2021), also shown in Figure 6.

The water contents as determined by TGA for samples of Winchcombe in this study were 12.4–13.3 wt %. As water content was measured using this method for samples which had their bulk mineralogy determined by PSD-XRD, either in this study or in King et al. (2022), we can correlate water abundance with phyllosilicate abundances (Figure 7). Also shown on this figure are the water contents as derived by Karl Fischer titration (13.8 wt%; this study), TGA without associated modal mineralogy (11.2 wt%; King et al., 2022) and by hydrogen pyrolysis (an average of 10.5 wt%; King et al., 2022).

Although the ranges of water content are all within the ranges of water abundances determined for CM chondrites previously (Figure 7; Garenne et al., 2014; King, Schofield, et al., 2021), the samples in this study show slightly higher values than previously measured for Winchcombe (King et al., 2022). Garenne et al. (2014) demonstrated that water abundances determined from TGA do show slightly higher values compared to other analytical methods, as other phases, such as sulfides, carbonates, and organics decompose within the "phyllosilicate" temperature range. This accounts for the lower values of water content calculated for Winchcombe by hydrogen pyrolysis; however, the sample (BM.2022, M1-88) that was analyzed using the TGA in the King et al. (2022) study also shows lower water abundance. Although no mineralogy was determined for that sample, its mass loss in the "phyllosilicate ranges" of 200–400°C (2.2 wt%) and 400–770°C (9.0 wt%) are consistently slightly lower than the mass loss in the samples in this study (2.7–3.7 and 9.6–10.2 wt%, respectively), indicating a lower degree of aqueous alteration.

Additionally, the difference in mass loss observed in the 200–400°C range between this (2.7–3.7 wt%) and the King et al. (2022) study (2.2 wt%) is likely related to the timing of measurements. The sample in the King et al. (2022) study, BM.2022,M1-88, was measured on March 5, 2021, 5 days after the observed fireball, in comparison to the samples in this study which were measured between 2 and 5 months after the event. In the

TABLE 6. Percentage of total iron contained in each mineral phase established for room temperature Mössbauer spectra.

Sample	Cronst. Fe^{2+}	Cronst. tet. Fe^{3+}	Cronst. oct. Fe^{3+}	Serp. Fe^{2+}	Toch. Fe^{2+}	Magn. $Fe^{2.5+}$	Magn. Fe^{3+}	Fe^{3+}/Fe^{T}
BM.2022,M1-100	29.6	10.6	16.1	16.7	27.1	<LOD	<LOD	0.27
BM.2022,M3-27	34.2	8.2	18.2	14.6	24.8	<LOD	<LOD	0.26
BM.2022,M8-14	34	13.7	11.2	17.5	23.5	<LOD	<LOD	0.25
BM.2022,M3-4	30	9	19	23	17	2	1	0.30

Abbreviation: LOD, limit of detection.

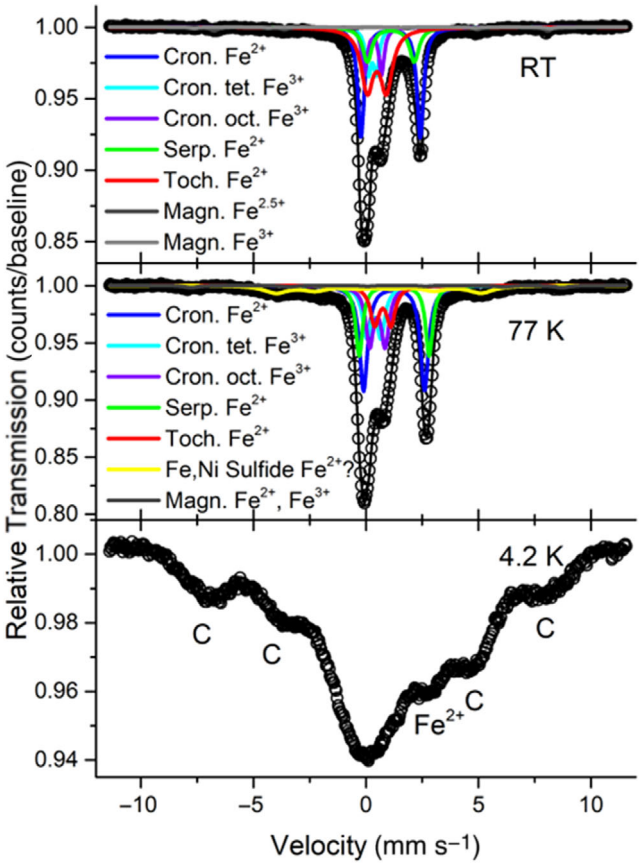

FIGURE 5. Temperature-dependent Mössbauer spectra of the powdered sample BM.2022,M3-4. Spectra were measured in transmission mode at room temperature (RT), 77, and 4.2 K. The black solid line represents the overall fit to the measured spectrum (black open circles) and is the sum of all subspectra (colored lines). Cronstedtite (Cron.) contains Fe^{2+} and Fe^{3+}, the latter in tetrahedral (tet.) and octahedral (oct.) coordination. Serpentine (Serp.) and tochilinite (Toch.) contain Fe^{2+}. The RT and 77 K spectra also reveal magnetite (Magn.). The 77 K spectrum shows a potential Fe,Ni sulfide (sulf.) phase. In the 4.2 K spectrum, peaks 1, 2, 5, and 6 of a sextet corresponding to magnetically ordered cronstedtite (C) are indicated, as well as the high velocity peak of an Fe^{2+} doublet.

case of BM.2022,M2-41 and BM.2022,M1-91, the samples were removed from their desiccator and subsampled for other analyses prior to the TGA measurements, increasing their exposure to the terrestrial environment. The 200–400°C range is associated not only with the dehydration of phyllosilicates but also the dehydroxylation of Fe-(oxy) hydroxides, which in meteorites are usually assumed to be the result of terrestrial contamination and modification. Adsorbed terrestrial water can also be dehydrated in this temperature range and the higher mass loss observed between 200 and 400°C in this study may be an effect of the prolonged time between the meteorite recovery and the measurements, resulting in higher abundances of terrestrially adsorbed water: approximately 0.5–1.5 wt%. The fact that there is not a clear increase in mass loss in the 200–400°C region between the samples measured 2 and 5 months after the recovery (Table 3; 2.7–3.7 wt%) indicates the terrestrial contamination likely effected the meteorite quickly, with these phases forming and affecting results within the first months. It is clear that periodic measurements of water abundance Winchcombe are required over the following years to evaluate whether the effect of terrestrial exposure further increases apparent water content as measured by TGA, as this will have implications for other historic carbonaceous chondrite falls and returned samples (DuFresne & Anders, 1962).

Element Composition

Evaluating the bulk chemistry of Winchcombe is an effective way to confirm the classification of the meteorite as a CM chondrite, and as major and trace element chemistry was presented in King et al. (2022), we can directly compare data from three bulk sample analyses. Figure 3a reveals that the bulk chemistry of Winchcombe is that of a CM chondrite, as its composition is very similar to the CM2 chondrites Murchison and Paris. Figure 3b,c also show that the data for Murchison and Paris agree well with data obtained by sector-field ICP-MS (Braukmüller et al., 2018; Hewins et al., 2014) and instrumental neutron activation analysis (INAA [Kallemeyn & Wasson, 1981]).

The chemical composition determined for Winchcombe, Murchison, and Paris also agree well with the CM reference data of Lodders (2021) and Braukmüller et al. (2018) (Figure 3a). However, the

TABLE 7. Mössbauer parameters of the 77 K spectrum of sample BM.2022,M3-4.

Mineral phase	Fe ox. state and coordination	δ (mm s^{-1})	ΔE_Q (mm s^{-1})	B_{hf} (T)	Γ (HWHM) (mm s^{-1})	Area (%)
Cronstedtite	Fe^{2+}	1.25	2.72	–	0.22	29
	Fe^{3+} tetrahedral	0.35	0.64	–	0.22	14
	Fe^{3+} octahedral	0.51	0.69	–	0.21	16
Serpentine	Fe^{2+}	1.26	3.12	–	0.19	17
Tochilinite	Fe^{2+}	0.75	0.72	–	0.24	12
Fe,Ni sulfide	Fe^{2+}	0.47	0.09	28.3	0.64	12
Magnetite	Fe^{2+}, Fe^{3+}	0.91	−0.45	51.0	0.37	2

Note: δ, isomer shift; ΔE_Q, quadrupole split; ε, quadrupole shift; B, magnetic hyperfine field; Γ, half width at half maximum for the relevant peak.

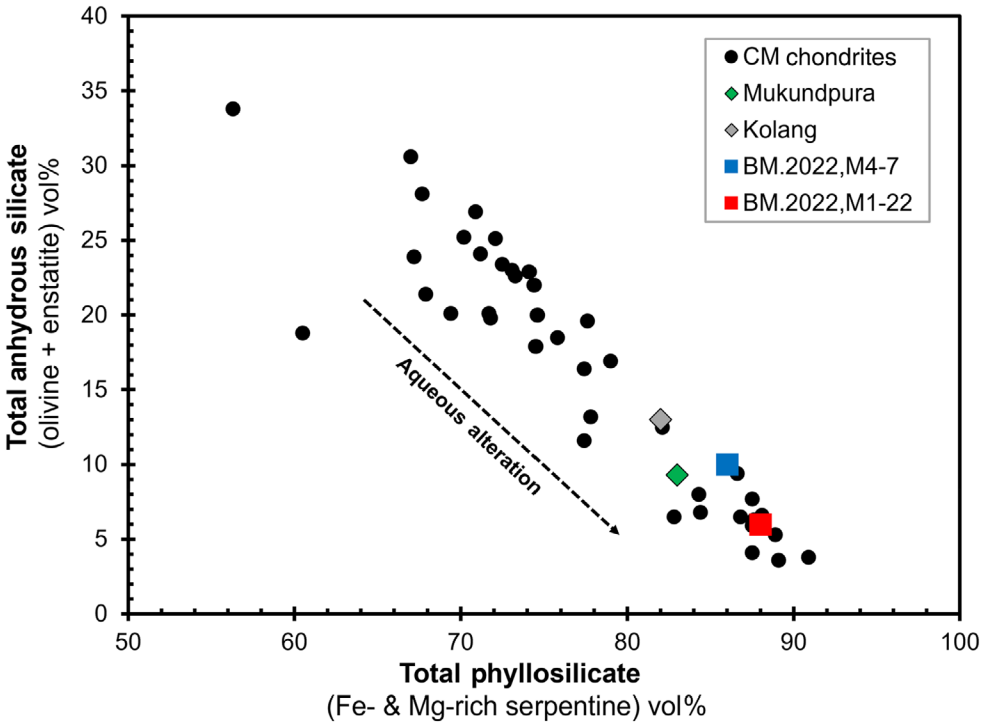

FIGURE 6. Total abundance of phyllosilicates (Fe- and Mg-rich serpentine) and anhydrous silicates (olivine and enstatite) measured in Winchcombe and CM chondrites using PSD-XRD. Data are from Howard et al. (2015), King et al. (2017), King, Bates, et al. (2021), and Krietsch et al. (2021).

refractory element abundances for W, Th, and Ir in Winchcombe, Murchison, and Paris are about 10%–25% lower than the reference values of Lodders (2021) and the W abundances for Murchison and Paris are also about 20% lower than those reported by Braukmüller et al. (2018). These observations may indicate some method-related biases. For example, Braukmüller et al. (2018) used the same calibration solution for Ir as in this study and reported similar low Ir values (Figure 3b, c). Our Ir value for Murchison is only 6% lower than the 0.569 μg g^{-1} reported by Fischer-Gödde et al. (2010) using the robust isotope dilution method. Further investigation into the potential cause of the variation in Ir abundances is required.

King et al. (2022) measured the chemical composition of two Winchcombe samples; BM.2022,M2-41 and BM.2022,M1-91. They observed an enrichment of the elements Ba, La, Ce, Dy, Ho, and Er in BM.2022,M2-41 when compared to other CM chondrites, attributing it to a refractory inclusion in the sample. Of these elements, sample BM.2022,M1-97 measured in this study only shows an enrichment in Ba (although by less), suggesting it does not contain the same refractory phase. As discussed in other studies (Suttle et al., 2022), Winchcombe does show variations in lithology, and the differences between the results from King et al. (2022) and those presented here are likely down to meteorite heterogeneity. However, broadly the chemical

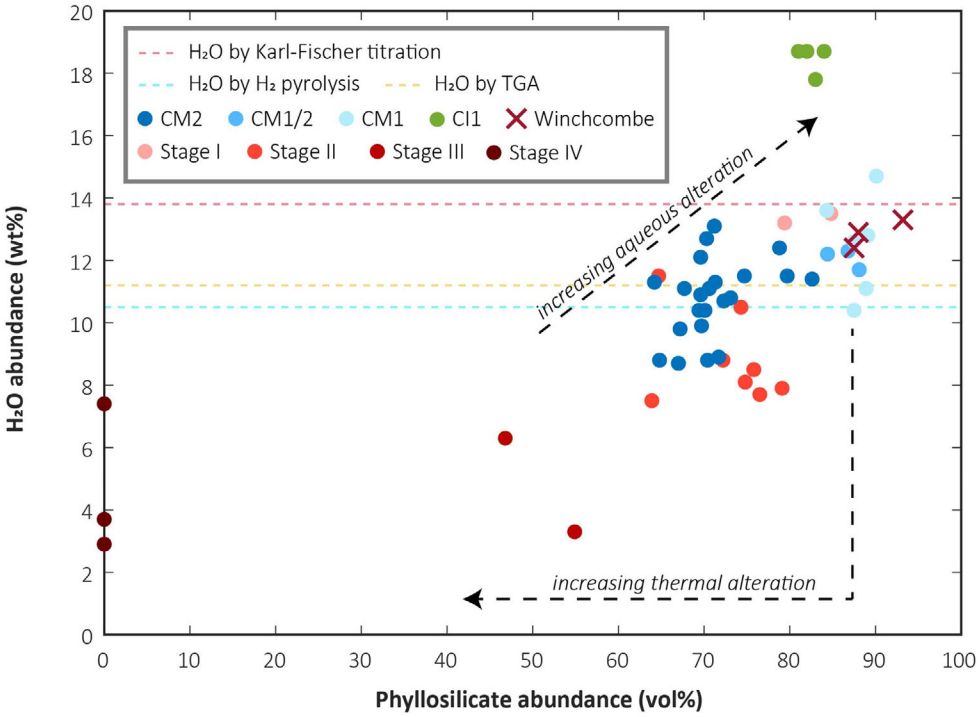

FIGURE 7. Measured H_2O abundances plotted against phyllosilicate abundance. Stages here refer to thermally altered CM chondrites according to the heating scale established by Nakamura (2005). The dashed colored lines represent water abundances for Winchcombe from Karl-Fischer titration (red), H_2 pyrolysis (blue), and TGA without modal mineralogy (yellow). The latter two of these data sets are from King et al. (2022). Increasing aqueous alteration causes both an increase in phyllosilicate and measured H_2O abundance. Increasing thermal metamorphism first causes a decrease in measured H_2O abundance as phyllosilicates are dehydrated into a "disordered phyllosilicate phase," before being recrystallized into secondary silicates, resulting in a drop in phyllosilicate abundance (e.g., King, Schofield, et al., 2021). CM data are from Bates et al. (2020), King et al. (2020), and King, Mason, et al. (2021); CI1 data are from King, Schofield, et al. (2015) and (King, Solomon, et al., 2015). Thermally altered CMs from stage I to stage IV data are from King, Schofield, et al. (2021), King, Russell, et al. (2019), and Lee et al. (2016).

compositions of all Winchcombe samples are very similar.

However, Figure 3a does reveal some additional minor deviations of BM.2022,M1-97 from typical CM chondrites, shown by the elemental composition of Paris and Murchison also measured here. Variations of the fluid mobile elements Ba, Na, and Cs may be due to heterogeneities induced by aqueous alteration on the parent body. Although all three meteorites measured here are CM chondrites, they show differing degrees of aqueous alteration, with Paris being among the least-altered CM chondrites with a PSF petrologic type of ~1.7 (Hewins et al., 2014; Krietsch et al., 2021), Murchison having a PSF petrologic type of ~1.5 (Howard et al., 2015), and Winchcombe being one of the more aqueously altered CM chondrites. The enrichment of Ba and Na in the Winchcombe sample when compared to other CM chondrites, both falls and finds (Braukmüller et al., 2018) may be additionally down to the low levels of terrestrial alteration in the Winchcombe samples, even compared to other CM chondrite falls, as a result of its rapid recovery. For example, Na has been found to become depleted during the process of evaporite formation during terrestrial weathering and by exposure to rainfall before recovery of meteorite falls (Bland et al., 2006; Haack et al., 2012). Additional differences between the CM chondrites analyzed here include the Mg-normalized moderately volatile elements P to Ga (condensation temperature range from 1230 to 970 K), which are consistently enriched by ~×1.04–1.09 in Winchcombe compared to Murchison and Paris. However, this enrichment is subtle and within the range of previously measured CM chondrites (Braukmüller et al., 2018).

The abundances of Hg in the Sun and in CI chondrites are not well constrained due to unreliable determinations of solar Hg abundances and probably due to contamination of Hg in CI chondrites (Lodders, 2003). Lodders (2021) reported a CI chondrite reference value of 288 ± 140 ng g^{-1}. Beer and Macklin (1985) determined the Hg abundance in the Sun based on models of stellar nucleosynthesis. Their data translate into a CI chondrite

reference value of 258 ± 30 ng g^{-1} (Anders & Grevesse, 1989; Lauretta et al., 1999). However, much higher Hg abundances between 1000 and 240,000 ng g^{-1} have frequently been reported, especially for the CI chondrite Orgueil, but also for Ivuna, Alais, and Tonk (compilation by Lauretta et al., 1999; Meier et al., 2016; Moynier et al., 2020; Palme & Zipfel, 2022; Wiederhold & Schönbächler, 2015). More recent reports for CM chondrites range from only 50 ng g^{-1} for Jbilet Winselwan, intermediate values between 221 and 408 ng g^{-1} for Murchison as well as higher Hg abundances of 2570 ng g^{-1} again for Murchison and 11,800 ng g^{-1} for Paris (Lauretta et al., 2001; Meier et al., 2016; Moynier et al., 2020). Lauretta et al. (2001), Wiederhold and Schönbächler (2015), Meier et al. (2016), and Moynier et al. (2020) argued that Hg abundances in their samples were not strongly affected by terrestrial contamination. While we are not able to completely resolve the issue of terrestrial Hg contamination of chondrites, Winchcombe provides an opportunity to obtain Hg abundances from a fresh fall where pervasive Hg contamination is extremely unlikely. Furthermore, we compare the Hg abundance in Winchcombe with that predicted from moderately volatile element abundances.

Moderately volatile elements with half condensation temperatures (T_C) between 800 and 500 K are depleted to the same extent relative to CI chondrites for a given carbonaceous chondrite group and have been referred to as plateau volatile elements (Braukmüller et al., 2018). For CM chondrites, the Mg and CI chondrite normalized depletion factor for plateau volatile elements is 0.49 (recalculated from the data in this study, see Ag to Tl in Figure 3a). Mercury is considered as a moderately volatile element (Palme et al., 2014), but its T_C is estimated at 258 and 240 K (Lodders, 2003; Wood et al., 2019), which makes Hg much more volatile than the plateau volatile elements of Braukmüller et al. (2018). A key question, therefore, is whether Hg behaves like a plateau volatile element in hydrated carbonaceous chondrites. If Hg were depleted in CM2 chondrites by the same factor as the plateau volatile elements (0.49), the Hg abundance ranges for CM chondrites can be predicted using the equation:

$$Hg_{CM} = 0.49 \times (Mg_{CM}/Mg_{CI}) \times Hg_{CI}$$

where Mg_{CI} is taken from Lodders (2021) and Mg_{CM} from this study. The predicted Hg_{CM} ranges are 137–173 ng g^{-1} based on Hg_{CI} values from Beer and Macklin (1985) and 89–258 ng g^{-1} for Hg_{CI} values from Lodders (2021).

Assuming that the above CI reference values are correct within their uncertainty, the value of 58.1 ± 0.5 ng g^{-1} Hg determined for our Winchcombe sample falls below the ranges predicted for CMs and therefore suggests that Hg can be more depleted in CM chondrites than usually observed for plateau volatile elements. Either Hg was initially more strongly depleted than the plateau volatile elements or it was affected by secondary processes. Meier et al. (2016) reasonably ascribed the systematically lower Hg contents in hot desert meteorites, including the CM chondrite Jbilet Winselwan, to them having experienced high equilibrium temperatures in the hot desert environment. This is obviously not the case for Winchcombe, which experienced temperatures of ~2°C on the night of the 28th of February, before being collected the next morning (Russell et al., 2022). Jbilet Winselwan also contains dehydrated lithologies (King, Russell, et al., 2019) and in dehydrated CM specimens, plateau volatile elements such as Zn are sometimes depleted (Mahan et al., 2018; Moriarty et al., 2009; Tonui et al., 2014). There is, however, no evidence for dehydration in any Winchcombe lithology (King et al., 2022; Suttle et al., 2022).

Based on the one Hg abundance measurement of 58 ng g^{-1} observed here for Winchcombe, we suggest that higher Hg abundances commonly observed in CI and CM chondrites, and in particular, those in the μg g^{-1} range are likely due to terrestrial Hg contamination. Provided that the CI chondrite reference values of Lodders (2021) and Beer and Macklin (1985) are accurate within their uncertainties, the low Hg content of Winchcombe suggests that Hg in hydrated carbonaceous chondrites does not behave like the plateau volatile elements with $T_C > 500$ K, but is more depleted. This single result does not preclude the possibility that Hg is heterogeneously distributed on carbonaceous chondrite parent bodies as envisaged by Meier et al. (2016). More Hg abundance data from fresh chondrite falls and data from returned asteroid samples like from Ryugu and Bennu are required to better constrain the cosmochemical behavior of Hg.

Iron Minerals and Iron Oxidation States

Iron minerals and iron oxidation states record the effect of aqueous alteration on meteorite parent bodies. The evolution of organic compounds during this alteration is affected by iron minerals and iron redox processes (Schröder et al., 2016). For example, metallic iron can act as a catalyst for organic chemistry (Brearley, 2021); iron sulfide mineral surfaces can act as templates for complex organic compounds (Wächtershäuser, 1992); and reactive iron mineral phases aide the preservation of organic compounds (Bonsall et al., 2022; Lalonde et al., 2012). We used Mössbauer spectroscopy (e.g., Gütlich & Schröder, 2012) to determine the bulk iron mineral phases and iron

oxidation states of the Winchcombe meteorite. Low-temperature Mössbauer spectra were obtained to look for magnetic transitions of potential (super)paramagnetic mineral phases that would indicate the presence of reactive iron species.

The temperature-dependent transmission spectra of the powdered sample BM.2022,M3-4 (Figure 5) are similar to others reported for CM2 chondrites: Mighei (Roy-Poulsen et al., 1981), Murchison (Burns & Fisher, 1994; Roy-Poulsen et al., 1981), Cold Bokkeveld (Burns & Fisher, 1990), and Mukundpura (Dixit et al., 2019; Tripathi et al., 2018). Almost 60% of iron is in the phyllosilicate mineral cronstedtite. Cronstedtite undergoes magnetic ordering below ~10 K (Burns & Fisher, 1994) and this is observed in the 4.2 K spectrum (Figure 5). Tochilinite contains approximately 25% of the iron, and another ferrous doublet was attributed to Fe-bearing serpentine. Magnetite occurs just above the detection limit of 2% total iron in the room temperature and 77 K spectra of sample BM.2022,M3-4. The iron-bearing phases identified in BM.2022,M3-4 through Mössbauer spectroscopy are consistent with the mineral phases identified qualitatively in XRD patterns of the same sample.

The tochilinite structure, $6Fe_{1-x}S•5(Mg,Fe)(OH)_2$, accommodates most of the iron in mackinawite-like FeS layers but can also accommodate some iron in brucite-like $(Mg,Fe)(OH)_2$ layers. In terrestrial tochilinites, iron in the mackinawite layers shows as a singlet in Mössbauer spectra (Chistyakova et al., 2005, 2006), analogous to stoichiometric mackinawite (Schröder et al., 2020). However, Burns and Fisher (1994) found that tochilinite in the Murchison meteorite is represented by a doublet in Mössbauer spectra, and we find the same for Winchcombe. Burns and Fisher (1994) argue that vacancies and Ni substitution in the mackinawite-like layers result in Fe:S significantly below the 1:1 stoichiometry, which is required for a singlet to appear in Mössbauer spectra (Schröder et al., 2020). The parameters we obtained for the tochilinite doublet in the Winchcombe spectra—$\delta = 0.49$ mm s^{-1} and $\Delta E_Q = 0.89$ mm s^{-1} at room temperature (Table 5); $\delta = 0.75$ mm s^{-1} and $\Delta E_Q = 0.72$ mm s^{-1} at 77 K (Table 7)—are comparable to those reported by Burns and Fisher (1994). The parameters differ significantly from parameters reported for brucite: $\delta = 1.15$–1.16 mm s^{-1} and $\Delta E_Q = 2.93$–2.94 mm s^{-1} at room temperature (Blaauw et al., 1979), therefore excluding that the doublet is the result of Fe in brucite layers. Any Fe in brucite-like layers would be below the detection limit.

An additional magnetically ordered phase appears in the 77 K spectrum (Figure 5). The internal magnetic field with $B_{hf} = 28$ T is close to that for metallic (Fe,Ni), but its isomer shift is too large ($\delta = 0.47$ mm s^{-1}; Table 7). This isomer shift would be consistent with a superparamagnetic iron (hydr)oxide phase of low crystallinity. Such a phase has been reported for Murchison by Madsen et al. (1988), but they observed a much larger magnetic splitting. We therefore attribute this additional phase to an (Fe,Ni) sulfide phase. We were not able to identify any peaks diagnostic of sulfides in the XRD pattern of BM.2022,M3-4, indicating that if this phase is present, it has a low abundance (Figure 2).

Mossbauer spectra are generally unable to detect a mineral phase if it contains <2% of total iron within a sample. The Mössbauer spectra showed no evidence for metallic Fe in any of the Winchcombe subsamples and although the abundance of metal in CM chondrites is generally low (e.g., Rubin et al., 2007), the sensitivity of the Mossbauer technique coupled with the lack of detection of metal indicates there is only trace amounts of metal in this sample of Winchcombe. We conclude that most metallic Fe originally present has been altered. As with the previous results, this is consistent with the absence of any metallic Fe peaks in the XRD patterns of any Winchcombe subsamples (Figure 1 and King et al., 2022). We additionally did not find any features consistent with Fe-bearing olivine in the Mössbauer spectra. The olivine identified with other methods must therefore be forsteritic, and most olivine (in particular the Fe-bearing compositions) has been altered.

Ferric Fe is almost exclusively hosted in cronstedtite with a minor contribution from magnetite. Ferric Fe abundances range from 25% to 30% of total iron (Table 6). This is significantly lower than the values between 49% and 71% reported for other CM2 chondrites (Bland et al., 2008; Roy-Poulsen et al., 1981; Sephton et al., 2004; Tripathi et al., 2018). However, these authors evaluated ferric Fe as a paramagnetic phase which would have included tochilinite, which we evaluated as a separate phase.

Reflectance Spectroscopy

In this study, we determined water content using TGA for two samples of the Winchcombe meteorite (Table 3) for which near- and mid- infrared (NIR and MIR) reflectance spectra and modal mineralogy were presented in King et al. (2022). The positions of features in the spectra of Winchcombe can be compared to other meteorite spectra to give an indication of degree of aqueous alteration. Bates et al. (2020) showed a number of MIR spectral parameters could be related to mineralogy determined through PSD-XRD, and therefore that these parameters were a method to quantify the degree of aqueous alteration. To determine spectral parameters, we used the same methodology as in

Bates et al. (2020) and Bates et al. (2021). We established the position of the OH− stretching feature near 3 μm, the Christiansen feature, and the transparency feature (Table 8).

Previously, the OH− stretching vibrational feature near 3 μm has been used to estimate water contents from both laboratory spectra of meteorites and remote observations of asteroids. As we have water abundances determined through TGA for BM.2022,M1-91 and BM.2022,M2-41 in this study, this provides an interesting comparison. Sato et al. (1997) and Rivkin et al. (2003) established a method of obtaining a H/Si ratio, and equivalent water content from spectral observations of asteroids and meteorites, using the ratio of the reflectance of spectra at 2.9 μm to the value at 2.5 μm, and the ratio of the reflectance of spectra at 3.2 μm to the value at 2.5 μm (eqs. 1 and 2 in Rivkin et al., 2003). These values can be combined with a bulk SiO_2 concentration, which is also quoted in the King et al.'s (2022) study for the same samples, to obtain equivalent water abundance (eq. 3 in Rivkin et al., 2003). Rivkin et al. (2003) found the difference between water content calculated from the laboratory spectra of meteorites and measured water content was up to 2.7%. Using this method applied to the spectra from King et al. (2022), we obtain an equivalent water content of 6.0% for sample BM.2022,M1-91 and 5.6% for sample BM.2022,M2-41.

Beck et al. (2021) expanded on this methodology to establish a relationship between the band depth of reflectance spectra (normalized to unity at 2.6 μm) at 2.75 and 2.80 μm to water abundance. Their calculation works for meteorites which had their spectra collected both without heating and with heating to 80–100°C to drive off adsorbed terrestrial water. Using their method, we calculated water contents of 10.5 and 9.5 wt% from the spectra of BM.2022,M1-91 and BM.2022,M2-41, respectively. The second method seems to provide more accurate values of water abundance, although still lower than the measured values of 12.4 and 13.3 wt%.

As described earlier, the higher estimated water content established from TGA could be due to the other phases which decompose in the 'phyllosilicate temperature range', such as sulfides, carbonates, and organics. These minerals do not contribute to the OH− stretching feature near 3 μm and so would not contribute to any estimations of water content calculated using spectral parameters. However, terrestrially adsorbed water would contribute to the −OH stretching feature, and therefore to calculations of water abundance. This is especially true in the case of the Winchcombe samples as they were not heated to drive off any terrestrial components prior to any spectra being collected (King et al., 2022). From TGA measurements of these samples, we know that there is approximately 2.7–3.0 wt% terrestrial water present in the Winchcombe samples. Garenne et al. (2014) describe this water as weakly bonded H_2O, both adsorbed and in mesopores. If this water is molecular H_2O, then it should contribute to the broad 3 μm feature at wavelengths of 3.10 μm (Gaffey et al., 1993), as opposed to 2.70–3.00 μm which is typically observed for the OH− in phyllosilicates. This could mean molecular H_2O does not contribute to the calculation derived by Beck et al. (2021) which only uses band depths at 2.75 and 2.80 μm. However, it is clear that in order to validate this method for determining water abundance using spectral parameters, spectral measurements of Winchcombe should be taken after heating the samples to remove terrestrial water. Additionally, comparison between the spectra of Winchcombe and the spectra of samples returned from asteroids Bennu and Ryugu should further clarify the effect of terrestrial contamination on spectra.

TABLE 8. The positions of spectral features.

	BM.2022,M1-91	BM.2022,M2-41
OH− stretching feature (μm)	2.76 ± 0.01	2.74 ± 0.01
Christiansen feature (μm)	9.21 ± 0.02	9.13 ± 0.01
Transparency feature (μm)	11.83 ± 0.03	11.48 ± 0.01

Note: Uncertainty was established by varying the range over which the polynomial at the center of each figure was plotted, and errors are one standard deviation from the average. Spectra are from King et al. (2022).

The Christiansen and transparency features in the MIR for Winchcombe are consistent in position with previous measurements of the same spectral features in other CM chondrites prepared and measured in the same way (Bates et al., 2020; King, Mason, et al., 2021). As suggested by King et al. (2022), the difference in Christiansen position between the two Winchcombe samples correlates with differences in olivine abundances. The transparency feature is a reflectance maximum/emissivity minimum caused by volume scattering in optically thin, fine-particulate materials (<75 μm) (Cooper, 2002; Salisbury, 1993), which has been shown to shift in position with changes in the surrounding vibrational features (Bates et al., 2020, 2021; McAdam et al., 2015; Salisbury & Walter, 1989). Figure 8 shows the position of the transparency feature determined for the Winchcombe spectra presented in King et al. (2022) plotted against PSF petrologic type determined in the same study. Also plotted are the transparency feature position and petrologic type for a number of highly aqueously altered CM2, CM1, and CI1 chondrites (PSF petrologic type 1.1–1.5, Bates et al., 2020) and for four CM chondrites with a low

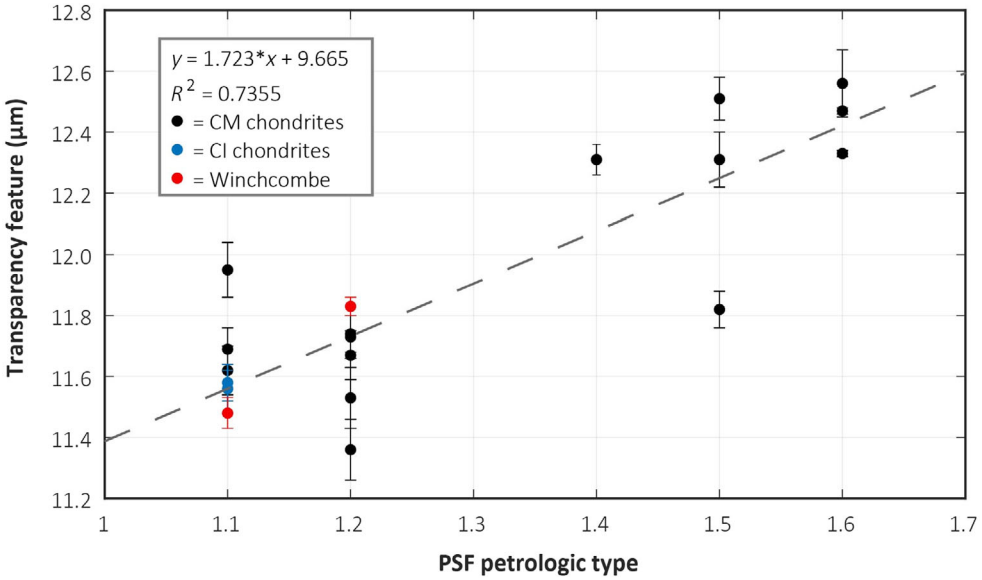

FIGURE 8. The position of the transparency feature against PSF petrologic type. CM data are from Bates et al. (2020) and King, Mason, et al. (2021). Error bars represent one standard deviation. The Winchcombe spectral parameters are shown in red.

degree of aqueous alteration (PSF petrologic type 1.4 to 1.6, King, Mason, et al., 2021). For both of these data sets, the modal mineralogy and spectra were collected using the same techniques as for the Winchcombe samples. The figure shows that the positions of the transparency feature in the Winchcombe spectra are consistent with highly aqueously altered CM chondrites, and that the transparency feature is a useful parameter for determining aqueous alteration. In order to validate this relationship, the positions of the transparency feature in the spectra of carbonaceous chondrites which have experienced more variable degrees of aqueous alteration need to be determined.

Relationship with Asteroid Surfaces

Ground-based telescopic observations of asteroids are hindered by the presence of water vapor in the terrestrial atmosphere, rendering the OH− stretching feature near 3 µm difficult to distinguish. It is for this reason that Rivkin et al. (2015) established a method of determining water abundance using the ratio of reflectance at wavelengths which are observable from the ground. In the previous section, we calculated the water abundance of Winchcombe using this method and the spectra presented in King et al. (2022), and although the values are lower than the measured values, we can still qualitatively compare the Winchcombe spectra to the asteroids from Rivkin et al. (2015) which produced similar calculated values of H/Si and water abundance (Figure 9).

Due to the gap in the remote observations, and in the cases of 168 Sibylla and 38 Leda, the low signal-to-noise ratio, it is challenging to determine a center for the OH− stretching feature for the asteroid observations, and to accurately and quantitatively evaluate whether Winchcombe could be an effective analog for these moderately aqueously altered asteroids. However, the figure does show that the calculations for water content established by Rivkin et al. (2015) are a useful tool for finding qualitatively similar asteroid and meteorite spectra. Additionally, based on our comparison between calculated and measured values of water abundance for Winchcombe, it is likely that the water content calculated for the surface of these asteroids is underestimated. This is supported somewhat by observations of asteroid 162173 Ryugu by the Hayabusa2 spacecraft that showed an OH− stretching feature which has a lower band depth than meteorite laboratory spectra. This resulted in a hypothesis that the asteroid surface was partially dehydrated by either shock heating, or radiative heating during travel closer to the sun in its past (Kitazato et al., 2019). However, initial investigations of samples returned from the asteroid have shown the Ryugu surface to share characteristics with CI chondrites (Yada et al., 2022). These meteorites are the most aqueously altered carbonaceous chondrite meteorites known and can contain 8–10 wt% water (as determined through H abundance and isotopic signature [Vacher et al., 2020]). The reason for the discrepancy between measurements of the samples and the spectral observations may well be down to our underestimation of the terrestrial influence

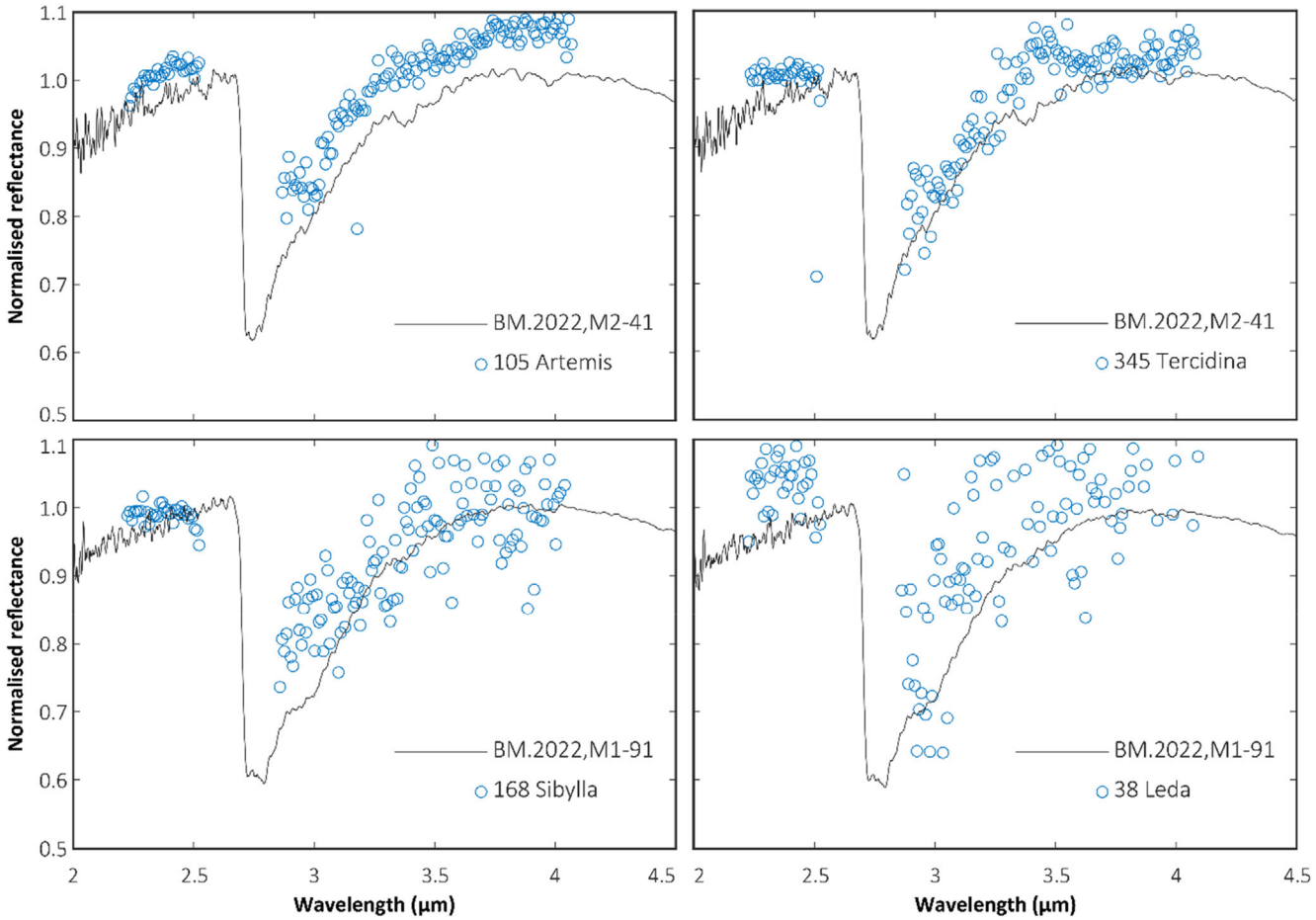

FIGURE 9. Comparison between the OH− stretching feature in the spectra of the Winchcombe samples BM.2022,M2,41 and BM.2022,M1-91, and asteroids 105 Artemis, 345 Tercidina, 168 Sibylla (Ch-type) and 38 Leda (Cgh-type). Artemis and Tercidina showed similar H/SI ratios to BM.2022,M2-41 (~1.25) and Sibylla and Leda showed similar H/Si to BM.2022,M1-91 (~1.4). The meteorite spectra have been normalized to a linear continuum fitted between 2.5 and 4.00 μm.

on the OH− stretching feature, although Noguchi et al. (2022) suggested that the weakened OH− stretching feature observed for Ryugu may be a result of space weathering. This study highlights the need for pristine samples uncontaminated by the terrestrial environment, in the form of both samples returned from asteroids, and fresh meteorite falls; samples that can be analyzed in the laboratory to ground-truth remote observations. This is particularly crucial for carbonaceous meteorites and asteroids (i.e., bodies that have been altered by water) as we want to determine their role in the delivery of volatiles to the terrestrial planets. To evaluate this, we need clarity on the effect of terrestrial processes on the samples we are comparing to remote data.

CONCLUSIONS

In this study, we show and discuss the bulk properties of the Winchcombe meteorite and give an interpretation of the degree of aqueous alteration. We determined modal mineralogy, water abundance, element composition, distribution of iron in different phases and iron oxidation state. The results show that Winchcombe is a highly altered CM chondrite, with a PSF petrologic type of ~1.2–1.3 and water contents of 12.4–13.8 wt%. Combining these with previous determinations of bulk modal mineralogy and water abundance, we get an average PSF petrologic type of 1.2 (2.1 in the Rubin et al. [2007] scale) and an average water abundance of 11.9 wt%.

The element composition is consistent with previous measurements of Winchcombe and with measurements of other CM chondrites such as Murchison and Paris. The Hg abundance of 58 ng g^{-1} is lower than expected for CM chondrites, if a depletion relative to CI and similar to other moderately volatile elements like Cd, In, or Tl is assumed. The bulk iron phases identified in Winchcombe include cronstedtite, tochilinite, and magnetite, with no

metallic Fe and low abundances of fayalitic olivine. This mineral assemblage is consistent with the mineralogy and high degree of aqueous alteration determined through other techniques.

We also evaluated the previously published spectra of Winchcombe, which shows positions of features similar to those observed in other spectra of highly aqueously altered CM chondrites. We use the spectra to evaluate H/Si ratio and water content in Winchcombe and find that spectral parameters tend to slightly underestimate the water abundance compared to abundances measured through methods such as TGA and Karl-Fischer titration. Nevertheless, calculated values of water abundance enable us to identify qualitatively similar asteroid spectra, which leads us to conclude that the water abundance on the surface of these asteroids is likely underestimated. It is clear that due to the quick recovery of the Winchcombe meteorite, it is comparable to samples returned from asteroid Ryugu by Hayabusa2 and those that will be returned from asteroid Bennu by OSIRIS-REx. However, in order to fully evaluate the effect of terrestrial contamination on meteorites, it will be necessary to investigate differences between Winchcombe and these returned samples.

Acknowledgments—This publication is part of the Winchcombe science team consortium, organized by the UK Fireball Alliance and conducted by the UK Cosmochemistry Network. The authors of this paper would like to thank the UK Fireball Alliance, its constituent networks (UK Fireball Network, SCAMP, UKMON, AllSky7, NEMATODE, GMN), international collaborators (FRIPON, Global Fireball Observatory, Desert Fireball Network, University of Western Ontario and University of Helsinki), and the meteor observation camera owners who participate in the UK Fireball Alliance network for their aid in observing the fireball and helping to predict its fall position. We would also like to thank the scientists and volunteers that participated in the UK Fireball Alliance led search and recovery of the Winchcombe meteorite, and the local community, who generously reported and donated meteorite finds and enabled the team to search the strewn field. STFC are acknowledged for supporting the "Curation and Preliminary Examination of the Winchcombe Carbonaceous Chondrite Fall" project (ST/V000799/1), and Natural History Museum staff for curatorial support. We additionally thank the Smithsonian Museum, Tim McCoy, and Glenn Macpherson for the Murchison meteorite sample used in this study, and Matthieu Gounelle at the MNHN Paris for the Paris meteorite sample. Some of this work was carried out in laboratories run by Jens Najorka and Carsten Münker and we are grateful for their support. HCB and AJK are funded by UK Research and Innovation (UKRI) grant MR/T020261/1. CS and EB thank STFC for support via a training grant quota studentship (ST/V50709X/1). KS, RC, and NEB thank STFC for support via grants ST/S000461/1 and ST/W000938/1.

Data Availability Statement—The data that support the findings of this study are available from the corresponding author upon reasonable request.

Editorial Handling—Dr. Michael Zolensky.

REFERENCES

Alexander, C. M. O'D., Fogel, M., Yabuta, H., and Cody, G. D. 2007. The Origin and Evolution of Chondrites Recorded in the Elemental and Isotopic Compositions of their Macromolecular Organic Matter. *Geochimica et Cosmochimica Acta* 71: 4380–403.

Alexander, C. M. O'D., Greenwood, R. C., Bowden, R., Gibson, J. M., Howard, K. T., and Franchi, I. A. 2018. A Mutli-Technique Search for the most Primitive CO Chondrites. *Geochimica et Cosmochimica Acta* 221: 406–20.

Anders, E., and Grevesse, N. 1989. Abundances of the Elements: Meteoritic and Solar. *Geochimica et Cosmochimica Acta* 53: 197–214.

Bates, H. C., Donaldson, H. K. L., King, A. J., Bowles, N. E., and Russell, S. S. 2021. A Spectral Investigation of Aqueously and Thermally Altered CM, CM-An, and CY Chondrites under Simulated Asteroid Conditions for Comparison with OSIRIS-REx and Hayabusa2 Observations. *Journal of Geophysical Research: Planets* 126: 1–30.

Bates, H. C., King, A. J., Donaldson, H. K. L., Bowles, N. E., and Russell, S. S. 2020. Linking Mineralogy and Spectroscopy of Highly Aqueously Altered CM and CI Carbonaceous Chondrites in Preparation for Primitive Asteroid Sample Return. *Meteoritics & Planetary Science* 55: 77–101.

Beck, P., Eschrig, J., Potin, S., Prestgard, T., Bonal, L., Quirico, E., and Schmitt, B. 2021. "Water" Abundance at the Surface of C-Complex Main-Belt Asteroids. *Icarus* 357: 114125.

Beer, H., and Macklin, R. L. 1985. 198,199,200,201,202,204Hg (n,γ) Cross Sections and the Termination of s-Process Nucleosynthesis. *Physical Review C* 32: 738–55.

Benedix, G. K., Leshin, L. A., Farquhar, J., Jackson, T., and Thiemens, M. H. 2003. Carbonates in CM2 Chondrites: Constraints on Alteration Conditions from Oxygen Isotopic Compositions and Petrographic Observations. *Geochimica et Cosmochimica Acta* 67: 1577–88.

Bischoff, A., Alexander, C. M. O'D., Barrat, J.-A., Burkhardt, C., Busemann, H., Degering, D., Di Rocco, T., et al. 2021. The Old, Unique C1 Chondrite Flensburg—Insight into the First Processes of Aqueous Alteration, Brecciation, and the Diversity of Water-Bearing Parent Bodies and Lithologies. *Geochimica et Cosmochimica Acta* 293: 142–86.

Blaauw, C., Stroink, G., Leiper, W., and Zentilli, M. 1979. Crystal-Field Properties of Fe in Brucite $Mg(OH)_2$. *Physics Status Solidi (B)* 92: 639–43.

Bland, P. A., Berry, F. J., Cadogan, J. M., Howard, K. T., and Cressey, G. 2008. Fe-Bearing Mineral Abundance in

Primitive Chondrites by Mössbauser Spectroscopy. In *71st Annual Meteoritical Society Meeting*, abstract number 5304.
Bland, P. A., Cressey, G., and Menzies, O. N. 2004. Modal Mineralogy of Carbonaceous Chondrites by X-Ray Diffraction and Mössbauer Spectroscopy. *Meteoritics & Planetary Science* 39: 3–16.
Bland, P. A., Zolensky, M. E., Benedix, G. K., and Sephton, M. A. 2006. Weathering of Chondritic Meteorites. *Meteorites and the Early Solar System II* 1: 853–67.
Bonsall, E., McHugh, M., Lerman, H., Hutchinson, I., and Schröder, C. 2022. Reactive Iron Mineral Phases May Preserve Organic Carbon on Mars: Implications for Raman Spectroscopy. *53rd Lunar and Planetary Science Conference*.
Braukmüller, N., Wombacher, F., Hezel, D. C., Escoube, R., and Münker, C. 2018. The Chemical Composition of Carbonaceous Chondrites: Implications for Volatile Element Depletion, Complementarity and Alteration. *Geochimica et Cosmochimica Acta* 239: 17–48.
Brearley, A. J. 2021. Nanophase Iron Carbides in Fine-Grained Rims in CM2 Carbonaceous Chondrites: Formation of Organic Material by Fischer–Tropsch Catalysis in the Solar Nebula. *Meteoritics & Planetary Science* 56: 108–26.
Browning, L. B., McSween, H. Y., and Zolensky, M. E. 1996. Correlated Alteration Effects in CM Carbonaceous Chondrites. *Geochimica et Cosmochimica Acta* 96: 2621–33.
Burns, R. G., and Fisher, D. S. 1990. *Pre-Terrestrial Oxidation Products in Carbonaceous Meteorites Identified by Mossbauer Spectroscopy*. NASA, Washington, Reports of Planetary Geology and Geophysics Program.
Burns, R. G., and Fisher, D. S. 1994. Nanophase Mixed-Valence Iron Minerals in Meteorites Identified by Cryogenic Mössbauer Spectroscopy. *Hyperfine Interactions* 91: 571–6.
Chistyakova, N. I., Gubaidulina, T. V., and Rusakov, V. S. 2006. Mössbauer Investigations of Natural and Synthetic Tochilinite and Valleriite. *Czechoslovak Journal of Physics* 56: E123–31.
Chistyakova, N. I., Rusakov, V. S., Gubaidulina, T. V., and Kozerenko, S. V. 2005. Investigations of Sulfide Minerals with Layered Structure by Mössbauer Spectroscopy Methods. *Hyperfine Interactions* 166: 613–7.
Clayton, R. N., and Mayeda, T. K. 1984. The Oxygen Isotope Record in Murchison and Other Carbonaceous Chondrites. *Earth and Planetary Science Letters* 67: 151–61.
Cooper, B. L. 2002. Midinfrared Spectral Features of Rocks and their Powders. *Journal of Geophysical Research* 107: 1–17.
Cornell, R. M., and Schwertmann, U. 2003. *The Iron Oxides: Structure, Properties, Reactions, Occurrences and Uses*. Weinheim: Wiley-VCH.
Cressey, G., and Schofield, P. F. 1996. Rapid Whole-Pattern Profile-Stripping Method for the Quantification of Multiphase Samples. *Powder Diffraction* 11: 35–9.
Curtis, R. J., Bates, H. C., Warren, T. J., Shirley, K. A., Brown, E. C., King, A. J., and Bowles, N. E. 2023. Bidirectional Reflectance Distribution Function Measurements of the Winchcombe Meteorite Using the Visible Oxford Space Environment Goniometer. *Meteoritics & Planetary Science*, in press.
Dixit, A., Tripathi, R. P., and Bhandari, N. 2019. Glassy Magnetic Cronstedtite Signatures in Mukundpura CM2 Chondrite Based on Magnetic and Mössbauer Studies. *Meteoritics & Planetary Science* 54: 2902–7.
DuFresne, E. R., and Anders, E. 1962. On the chemical evolution of the carbonaceous chondrites. *Geochimica et Cosmochimica Acta* 26: 1085–113.
Fischer-Gödde, M., Becker, H., and Wombacher, F. 2010. Rhodium, Gold and Other Highly Siderophile Element Abundances in Chondritic Meteorites. *Geochimica et Cosmochimica Acta* 74: 356–79.
Fujia, W. 2018. Oxygen Isotopic Ratios of Primordial Water in Carbonaceous Chondrites. *Earth and Planetary Science Letters* 481: 264–72.
Fujiya, W., Sugiura, N., Hotta, H., Ichimura, K., and Sano, Y. 2012. Evidence for the Late Formation of Hydrous Asteroids from Young Meteoritic Carbonates. *Nature Communications* 3: 1–6.
Gaffey, S. J., McFadden, L. A., Nash, D., and Pieters, C. M. 1993. Ultraviolet, Visible, and near-Infrared Reflectance Spectroscopy: Laboratory Specta of Geologic Materials. In *Remote Geochemical Analysis: Elemental and Mineralogical Composition*, edited by C. M. Pieters, and P. A. Englert, 43–79. Cambridge: Cambridge University Press.
Garenne, A., Beck, P., Montes-Hernandez, G., Chiriac, R., Toche, F., Quirico, E., Bonal, L., and Schmitt, B. 2014. The Abundance and Stability of "Water" in Type 1 and 2 Carbonaceous Chondrites (CI, CM and CR). *Geochimica et Cosmochimica Acta* 137: 93–112.
Grady, M. M., Graham, A. L., Barber, D. J., Aylmer, D., Kurat, G., Ntaflos, T., Ott, U., Palme, H., and Spettel, B. 1987. Yamato-82042: An Unusual Carbonceous Chondrite with CM Affinities. *Memoirs of National Institute of Polar Research Special Issue* 46: 162–78.
Greenwood, R. C., Findlay, R., Martins, R., Steele, R. C. J., Rehkämper, M., Shaw, K., Savage, P. S., et al. 2022. Formation and Early Aqueous Alteration of the CM2 Parent Body: O, Cr, Cd, Si, Te, Ti and Zn Isotopic Evidence from the Winchcombe Chondrite Fall. *Meteoritics & Planetary Science (Winchcombe Special Issue)*.
Guo, W., and Eiler, J. M. 2007. Temperatures of Aqueous Alteration and Evidence for Methane Generation on the Parent Bodies of the CM Chondrites. *Geochimica et Cosmochimica Acta* 71: 5565–75.
Gütlich, P., and Schröder, C. 2012. Mössbauer Spectroscopy. In *Methods in Physical Chemistry*, 351–89. Weinheim: Wiley-VCH Verlag GmbH & Co., KGaA.
Haack, H., Grau, T., Bischoff, A., Horstmann, M., Wasson, J., Sørensen, A., Laubenstein, M., et al. 2012. Maribo-A New CM Fall from Denmark. *Meteoritics & Planetary Science* 47: 30–50.
Hanna, R. D., Hamilton, V. E., Haberle, C. W., King, A. J., Abreu, N. M., and Friedrich, J. M. 2020. Distinguishing Relative Aqueous Alteration and Heating among CM Chondrites with IR Spectroscopy. *Icarus* 346: 113760.
Hewins, R. H., Bourot-Denise, M., Zanda, B., Leroux, H., Barrat, J.-A., Humayun, M., Göpel, C., et al. 2014. The Paris Meteorite, the least Altered CM Chondrite So Far. *Geochimica et Cosmochimica Acta* 124: 190–222.
Howard, K. T., Alexander, C. M. O'D., Schrader, D. L., and Dyl, K. A. 2015. Classification of Hydrous Meteorites (CR, CM and C2 Ungrouped) by Phyllosilicate Fraction: PSD-XRD Modal Mineralogy and Planetesimal Environments. *Geochimica et Cosmochimica Acta* 149: 206–22.
Howard, K. T., Benedix, G. K., Bland, P. A., and Cressey, G. 2009. Modal Mineralogy of CM2 Chondrites by X-Ray

Diffraction (PSD-XRD). Part 1: Total Phyllosilicate Abundance and the Degree of Aqueous Alteration. *Geochimica et Cosmochimica Acta* 73: 4576–89.

Howard, K. T., Benedix, G. K., Bland, P. A., and Cressey, G. 2011. Modal Mineralogy of CM Chondrites by X-Ray Diffraction (PSD-XRD): Part 2. Degree, Nature and Settings of Aqueous Alteration. *Geochimica et Cosmochimica Acta* 75: 2735–51.

James, F. 2004. MINUIT Tutorial, Function Minimization. In *CERN Computing and Data Processing School*, 10–24. Pertisau.

Jenkins, L. E., Lee, M. R., Daly, L., King, A. J., Floyd, C. J., Martin, P.-E., Almeida, N. V., and Genge, M. J. 2022. Winchcombe: An Example of Rrapid Terrestrial Alteration in CM Chondrites. *Meteoritics & Planetary Science (Winchcombe Special Issue)*.

Jilly, C. E., Huss, G. R., Krot, A. N., Nagashima, K., Yin, Q. Z., and Sugiura, N. 2014. ^{53}Mn-^{53}Cr Dating of Aqueously Formed Carbonates in the CM2 Lithology of the Sutter's Mill Carbonaceous Chondrite. *Meteoritics & Planetary Science* 49: 2104–17.

Kallemeyn, G. W., and Wasson, J. T. 1981. The Compositional Classification of Chondrites—I. The Carbonaceous Chondrite Groups. *Geochimica et Cosmochimica Acta* 45: 1217–30.

Kerraouch, I., Kebukawa, Y., Bischoff, A., Zolensky, M. E., Wölfer, E., Hellmann, J. L., Ito, M., et al. 2022. Heterogeneous Nature of the Carbonaceous Chondrite Breccia Aguas Zarcas–Cosmochemical Characterization and Origin of New Carbonaceous Chondrite Lithologies. *Geochimica et Cosmochimica Acta* 334: 155–86.

King, A. J., Bates, H. C., Krietsch, D., Busemann, H., Clay, P. L., Schofield, P. F., and Russell, S. S. 2019. The Yamato-Type (CY) Carbonaceous Chondrite Group: Analogues for the Surface of Asteroid Ryugu? *Geochemistry* 79: 125531.

King, A. J., Bates, H. C., Schofield, P. F., and Russell, S. S. 2021. The Bulk Mineralogy and Water Contents of the Carbonaceous Chondrite Falls Kolang and Tarda. *52nd Lunar and Planetary Science Conference*, abstract number 1909.

King, A. J., Daly, L., Rowe, J., Joy, K. H., Greenwood, R. C., Devillepoix, H. A. R., Suttle, M. D., et al. 2022. The Winchcombe Meteorite, a Unique and Pristine Witness from the Outer Solar System. *Science Advances* 8: 46.

King, A. J., Mason, E., Bates, H. C., Schofield, P. F., Donaldson, H. K. L., Bowles, N. E., and Russell, S. S. 2021. Tracing the Earliest Stages of Hydrothermal Alteration on the CM Chondrite Parent Body. *Meteoritics & Planetary Science* 56: 1708–28.

King, A. J., Russell, S. S., Schofield, P. F., Humphreys-Williams, E. R., Strekopytov, S., Abernethy, F. A. J., Verchovsky, A. B., and Grady, M. M. 2019. The Alteration History of the Jbilet Winselwan CM Carbonaceous Chondrite: An Analog for C-Type Asteroid Sample Return. *Meteoritics & Planetary Science* 54: 521–43.

King, A. J., Schofield, P. F., Howard, K. T., and Russell, S. S. 2015. Modal Mineralogy of CI and CI-Like Chondrites by X-Ray Diffraction. *Geochimica et Cosmochimica Acta* 165: 148–60.

King, A. J., Schofield, P. F., and Russell, S. S. 2017. Type 1 Aqueous Alteration in CM Carbonaceous Chondrites: Implications for the Evolution of Water-Rich Asteroids. *Meteoritics & Planetary Science* 52: 1197–215.

King, A. J., Schofield, P. F., and Russell, S. S. 2021. Thermal Alteration of CM Carbonaceous Chondrites: Mineralogical Changes and Metamorphic Temperatures. *Geochimica et Cosmochimica Acta* 298: 167–90.

King, A. J., Solomon, J. R., Schofield, P. F., and Russell, S. S. 2015. Characterising the CI and CI-Like Carbonaceous Chondrites Using Thermogravimetric Analysis and Infrared Spectroscopy. *Earth, Planets and Space* 67: 198.

King, A. J., Zulmahilan, N. N. B., Schofield, P. F., and Russell, S. S. 2020. CM Chondrites from Multiple Parent Bodies: Evidence from Correlated Mineralogy and Cosmic-Ray Exposure Ages. *51st Lunar and Planetary Science Conference*, abstract number 1883.

Kiseeva, E. S., and Wood, B. J. 2015. The Effects of Composition and Temperature on Chalcophile and Lithophile Element Partitioning into Magmatic Sulphides. *Earth and Planetary Science Letters* 424: 280–94.

Kitazato, K., Milliken, R. E., Iwata, T., Abe, M., Ohtake, M., Matsuura, S., Arai, T., et al. 2019. The Surface Composition of Asteroid 162173 Ryugu from Hayabusa2 Near-Infrared Spectroscopy. *Science* 364: 272–5.

Klingelhöfer, G., Morris, R. V., Bernhardt, B., Rodionov, D., de Souza, P. A., Jr., Squryes, S. W., Foh, J., et al. 2003. Athena MIMOS II Mössbauer Spectrometer Investigation. *Journal of Geophysical Research: Planets* 108: 8067.

Kojima, H., Ikeda, Y., and Yanai, K. 1984. The Alteration of Chondrules and Matrices in New Antarctic Carbonaceous Chondrites. *Memoirs of National Institute of Polar Research, Special Issue* 35: 184–99.

Krietsch, D., Busemann, H., Riebe, M. E. I., King, A. J., Alexander, C. M. O'D., and Maden, C. 2021. Noble Gases in CM Carbonaceous Chondrites: Effect of Parent Body Aqueous and Thermal Alteration and Cosmic Ray Exposure Ages. *Geochimica et Cosmochimica Acta* 310: 240–80.

Lalonde, K., Mucci, A., Ouellet, A., and Gélinas, Y. 2012. Preservation of Organic Matter in Sediments Promoted by Iron. *Nature* 483: 198–200.

Lauretta, D. S., Devouard, B., and Buseck, P. R. 1999. The Cosmochemical Behavior of Mercury. *Earth and Planetary Science Letters* 171: 35–47.

Lauretta, D. S., Klaue, B., Blum, J. D., and Buseck, P. R. 2001. Mercury Abundances and Isotopic Compositions in the Murchison (CM) and Allende (CV) Carbonaceous Chondrites. *Geochimica et Cosmochimica Acta* 65: 2807–18.

Lee, M. R., Lindgren, P., King, A. J., Greenwood, R. C., Franchi, I. A., and Sparkes, R. 2016. Elephant Moraine 96029, a Very Mildly Aqueously Altered and Heated CM Carbonaceous Chondrite: Implications for the Drivers of Parent Body Processing. *Geochimica et Cosmochimica Acta* 187: 237–59.

Lentfort, S., Bischoff, A., Ebert, S., and Patzek, M. 2021. Classification of CM Chondrite Breccias—Implications for the Evaluation of Samples from the OSIRIS-REx and Hayabusa2 Missions. *Meteoritics & Planetary Science* 56: 127–47.

Lodders, K. 2003. Solar System Abundances and Condensation Temperatures of the Elements. *The Astrophysical Journal* 591: 1220–47.

Lodders, K. 2021. Relative Atomic Solar System Abundances, Mass Fractions, and Atomic Masses of the Elements and their Isotopes, Composition of the Solar Photosphere, and Compositions of the Major Chondritic Meteorite Groups. *Space Science Reviews* 217: 1–33.

Madsen, M. B., Mørup, S., Costa, T. V. V., Knudsen, J. M., and Olsen, M. 1988. Superparamagnetism in Primitive Meteorites. *Hyperfine Interactions* 41: 827–30.

Mahan, B., Moynier, F., Beck, P., Pringle, E. A., and Siebert, J. 2018. A History of Violence: Insights into Post-Accretionary Heating in Carbonaceous Chondrites from Volatile Element Abundances, Zn Isotopes and Water Contents. *Geochimica et Cosmochimica Acta* 220: 19–35.

McAdam, M. M., Sunshine, J. M., Howard, K. T., and Mccoy, T. M. 2015. Aqueous Alteration on Asteroids: Linking the Mineralogy and Spectroscopy of CM and CI Chondrites. *Icarus* 245: 320–32.

McSween, H. Y. 1979. Alteration in CM Carbonaceous Chondrites Inferred from Modal and Chemical Variations in the Matric. *Geochimica et Cosmochimica Acta* 43: 1761–70.

Meier, M. M. M., Cloquet, C., and Marty, B. 2016. Mercury (Hg) in Meteorites: Variations in Abundance, Thermal Release Profile, Mass-Dependent and Mass-Independent Isotopic Fractionation. *Geochimica et Cosmochimica Acta* 182: 55–72.

Moriarty, G. M., Rumble, I. D., and Friedrich, J. M. 2009. Compositions of Four Unusual CM or CM-Related Antarctic Chondrites. *Chemie der Erde—Geochemistry* 69: 161–8.

Moynier, F., Chen, J., Zhang, K., Cai, H., Wang, Z., Jackson, M. G., and Day, J. M. D. 2020. Chondritic Mercury Isotopic Composition of Earth and Evidence for Evaporative Equilibrium Degassing during the Formation of Eucrites. *Earth and Planetary Science Letters* 551: 116544.

Nakamura, T. 2005. Post-Hydration Thermal Metamorphism of Carbonaceous Chondrites. *Journal of Mineralogical and Petrological Sciences* 100: 260–72.

Noguchi, T., Matsumoto, T., Miyake, A., Igami, Y., Haruta, M., Saito, H., Hata, S., et al. 2022. A Dehydrated Space-Weathered Skin Cloaking the Hydrated Interior of Ryugu. *Nature Astronomy* 7: 170–81. https://doi.org/10.1038/s41550-022-01841-6.

Palguta, J., Schubert, G., and Travis, B. J. 2010. Fluid Flow and Chemical Alteration in Carbonaceous Chondrite Parent Bodies. *Earth and Planetary Science Letters* 296: 235–43.

Palme, H., Lodders, K., and Jones, A. 2014. Solar System Abundances of the Elements. In *Planets, Asteroids, Comets and the Solar System, Volume 2 of Treatise on Geochemistry*, edited by A. M. Davis, 2nd ed., vol. 2, 15–36. Oxford: Elsevier.

Palme, H., and Zipfel, J. 2022. The Composition of CI Chondrites and their Contents of Chlorine and Bromine: Results from Instrumental Neutron Activation Analysis. *Meteoritics & Planetary Science* 57: 317–33.

Rivkin, A. S., Davies, J. K., Johnson, J. R., Ellison, S. L., Trilling, D. E., Brown, R. H., and Lebofsky, L. A. 2003. Hydrogen Concentrations on C-Class Asteroids Derived from Remote Sensing. *Meteoritics & Planetary Science* 38: 1383–98.

Rivkin, A. S., Thomas, C. A., Howell, E. S., and Emery, J. P. 2015. The Ch-class Asteroids: Connecting a Visible Taxonomic Class to a 3 μm Band Shape. *The Astronomical Journal* 150: 198.

Roy-Poulsen, H., Larsen, L., Roy-Poulsen, N. O., Vistisen, L., and Knudsen, J. M. 1981. Meteorites and the Origin of Water and Reduced Carbon on the Earth. *Physica Scripta* 23: 1113–7.

Rubin, A. E., Trigo-Rodríguez, J. M., Huber, H., and Wasson, J. T. 2007. Progressive Aqueous Alteration of CM Carbonaceous Chondrites. *Geochimica et Cosmochimica Acta* 71: 2361–82.

Russell, S. S., King, A. J., Bates, H. C., Almeida, N. V., Greenwood, R. C., Daly, L., Joy, K. H., et al. 2022. Recovery and Curation of the Winchcombe (CM2) Meteorite. *Meteoritics & Planetary Science (Winchcombe Special Issue)*.

Salisbury, J. W. 1993. Mid-Infrared Spectroscopy: Laboratory Data. In *Remote Geochemical Analysis: Elemental and Mineralogical Composition*, 79–98. Cambridge: Cambridge University Press.

Salisbury, J. W., and Walter, L. S. 1989. Thermal Infrared (2.5–13.5 μm) Spectroscopic Remote Sensing of Igneous Rock Types on Particulate Planetary Surfaces. *Journal of Geophysical Research* 94: 9192–202.

Sato, K., Miyamoto, M., and Zolensky, M. E. 1997. Absorption Bands near Three Micrometers in Diffuse Reflectance Spectra of Carbonaceous Chondrites: Comparison with Asteroids. *Meteoritics & Planetary Science* 32: 503–7.

Schofield, P. F., Knight, K. S., Covey-Crump, S. J., Cressey, G., and Stretton, I. C. 2002. Accurate Quantification of the Modal Mineralogy of Rocks when Image Analysis is Difficult. *Mineralogical Magazine* 66: 189–200.

Schröder, C., Köhler, I., Muller, F. L. L., Chumakov, A. I., Kupenko, I., Rüffer, R., and Kappler, A. 2016. The Biogeochemical Iron Cycle and Astrobiology. *Hyperfine Interactions* 237: 1–14.

Schröder, C., Wan, M., Butler, I. B., Tait, A., Peiffer, S., and McCammon, C. A. 2020. Identification of Mackinawite and Constraints on its Electronic Configuration Using Mössbauer Spectroscopy. *Minerals* 10: 1090.

Sephton, M. A., Bland, P. A., Pillinger, C. T., and Gilmour, I. 2004. The Preservation State of Organic Matter in Meteorites from Antarctica. *Meteoritics & Planetary Science* 39: 747–54.

Suttle, M. D., Daly, L., Jones, R. H., Jenkins, L., Van Ginneken, M., Mitchell, J. T., Bridges, J. C., et al. 2022. The Winchcombe Meteorite—A Regolith Breccia from a Rubble-Pile CM Chondrite Asteroid. *Meteoritics & Planetary Science (Winchcombe Special Issue)*.

Tomeoka, K., and Buseck, P. R. 1985. Indicators of Aqueous Alteration in CM Carbonaceous Chondrites: Microtextures of a Layered Mineral Containing Fe, S, 0 and Ni. *Geochimica et Cosmochimica Acta* 49: 2149–63.

Tonui, E. K., Zolensky, M. E., Hiroi, T., Nakamura, T., Lipschutz, M. E., Wang, M.-S., and Okudaira, K. 2014. Petrographic, Chemical and Spectroscopic Evidence for Thermal Metamorphism in Carbonaceous Chondrites I: CI and CM Chondrites. *Geochimica et Cosmochimica Acta* 126: 284–306.

Tripathi, R. P., Dixit, A., and Bhandari, N. 2018. Characterization of Mukundpura Carbonaceous Chondrite. *Current Science* 114: 214–7.

Vacher, L., Piralla, M., Gounelle, M., Vacher, L. G., Bizzarro, M., and Marrocchi, Y. 2019. Thermal Evolution of Hydrated Asteroids Inferred from Oxygen Isotopes. *The Astrophysical Journal Letters* 882: L20.

Vacher, L. G., Piani, L., Rigaudier, T., Thomassin, D., Florin, G., Piralla, M., and Marrocchi, Y. 2020. Hydrogen in Chondrites: Influence of Parent Body Alteration and Atmospheric Contamination on Primordial Components. *Geochimica et Cosmochimica Acta* 281: 53–66.

Verdier-Paoletti, M. J., Marrocchi, Y., Avice, G., Roskosz, M., Gurenko, A., and Gounelle, M. 2017. Oxygen Isotope Constraints on the Alteration Temperatures of CM Chondrites. *Earth and Planetary Science Letters* 458: 273–81.

Verdier-Paoletti, M. J., Marrocchi, Y., Vacher, L. G., Gattacceca, J., Gurenko, A., Sonzogni, C., and Gounelle, M. 2019. Testing the Genetic Relationship between Fluid Alteration and Brecciation in CM Chondrites. *Meteoritics & Planetary Science* 54: 1692–709.

Visser, R., John, T., Whitehouse, M. J., Patzek, M., and Bischoff, A. 2020. A Short-Lived ^{26}Al Induced Hydrothermal Alteration Event in the Outer Solar System: Constraints from Mn/Cr Ages of Carbonates. *Earth and Planetary Science Letters* 547: 116440.

Wächtershäuser, G. 1992. Groundworks for an Evolutionary Biochemistry: The Iron-Sulphur World. *Progress in Biophysics and Molecular Biology* 58: 85–201.

Wiederhold, J. G., and Schönbächler, M. 2015. Mercury Concentrations and Hg Isotope Compositions of Chondrites and Eucrites. *46th Lunar and Planetary Science Conference*, abstract number 1841.

Wood, B. J., Smythe, D. J., and Harrison, T. 2019. The Condensation Temperatures of the Elements: A Reappraisal. *American Mineralogist* 104: 844–56.

Yada, T., Abe, M., Okada, T., Yogata, K., Miyazaki, A., Hatakeda, K., Kumagai, K., et al. 2022. Preliminary Analysis of the Hayabusa2 Samples Returned from C-Type Asteroid Ryugu. *Nature Astronomy* 6: 214–20.

Zolensky, M. E., Mittlefehldt, D. W., Lipschutz, M. E., Wang, M.-S., Clayton, R. N., Mayeda, T. K., Grady, M. M., Pillinger, C., and Barber, D. 1997. CM Chondrites Exhibit the Complete Petrologic Range from Type 2 to 1. *Geochimica et Cosmochimica Acta* 61: 5099–115.

SUPPORTING INFORMATION

Additional supporting information may be found in the online version of this article.

Figure S1 Mass loss and derivative of mass loss (DTG) curves for the two Winchcombe samples BM.2022,M1-22 (top panel) and BM.2022,M2-41 (bottom panel). Peaks in the DTG curves correspond to specific mineral phases dehydrating. Winchcombe shows significant mass loss between 200 and 770°C due to the dehydration and dehydroxylation of phyllosilicates; however, small amounts of Fe-(oxy)hydroxides, Fe-sulfides, and some organic matter may also contribute to mass loss in this region.

Figure S2 Backscatter Mössbauer spectra of three rock chips of the Winchcombe meteorite obtained with the miniaturized Mössbauer spectrometer MIMOS II over the velocity range ± 12 mm s^{-1}.